9748–9764 *Nucleic Acids Research, 2022, Vol. 50, No. 17* *Published online 27 August 2022*
https://doi.org/10.1093/nar/gkac730

Dichotomous *cis*-regulatory motifs mediate the maturation of the neuromuscular junction by retrograde BMP signaling

Robin Vuilleumier[1,*], Mo Miao[1], Sonia Medina-Giro[1], Clara-Maria Ell[2,3], Stephane Flibotte[1], Tianshun Lian[1], Grant Kauwe[4], Annie Collins[1], Sophia Ly[1], George Pyrowolakis[3], A. Pejmun Haghighi[4] and Douglas W. Allan[1,*]

[1]Department of Cellular and Physiological Sciences, University of British Columbia, Vancouver, British Columbia, V6T 1Z3, Canada, [2]Spemann Graduate School of Biology and Medicine (SGBM), University of Freiburg, Freiburg, 79104, Germany, [3]CIBSS - Centre for Integrative Biological Signaling Studies and Institute for Biology I, Faculty of Biology, Hilde Mangold Haus, Habsburgerstrasse 49, University of Freiburg, Freiburg, 79104, Germany and [4]Buck Institute for Research on Aging, Novato, CA 94945, USA

Received February 12, 2022; Revised July 20, 2022; Editorial Decision August 08, 2022; Accepted August 19, 2022

ABSTRACT

Retrograde bone morphogenetic protein (BMP) signaling at the *Drosophila* neuromuscular junction (NMJ) has served as a paradigm to study TGF-β-dependent synaptic function and maturation. Yet, how retrograde BMP signaling transcriptionally regulates these functions remains unresolved. Here, we uncover a gene network, enriched for neurotransmission-related genes, that is controlled by retrograde BMP signaling in motor neurons through two Smad-binding *cis*-regulatory motifs, the BMP-activating (*BMP-AE*) and silencer (*BMP-SE*) elements. Unpredictably, both motifs mediate direct gene activation, with no involvement of the BMP derepression pathway regulators Schnurri and Brinker. Genome editing of candidate *BMP-SE* and *BMP-AE* within the locus of the active zone gene *bruchpilot*, and a novel Ly6 gene *witty*, demonstrated the role of these motifs in upregulating genes required for the maturation of pre- and post-synaptic NMJ compartments. Our findings uncover how Smad-dependent transcriptional mechanisms specific to motor neurons directly orchestrate a gene network required for synaptic maturation by retrograde BMP signaling.

INTRODUCTION

In metazoans, transforming growth factor-beta (TGF-β) members play key roles in the developing and mature central nervous system (CNS) to orchestrate a wide variety of processes including neurogenesis, neuronal specification, synaptic growth as well as stability, neurotransmission, homeostasis and plasticity (1,2). Commensurate with its critical neuronal functions, deregulation of the TGF-β pathway is linked with multiple severe human neurological disorders (3,4). Despite these roles, the downstream molecular and transcriptional mechanisms regulated by neuronal TGF-β signaling remain largely unknown.

The *Drosophila* neuromuscular junction (NMJ) provides an ideal model for determining how TGF-β signaling coordinates complex synaptic functions and its downstream effector target genes. At the growing larval NMJ, bone morphogenetic proteins (BMPs), a branch of TGF-β ligands, trigger retrograde BMP signaling and downstream transcription in motor neurons that are essential for synaptic function and maturation (5–7). Secreted at the NMJ by muscle cells and motor neurons, the BMP ligand Glass bottom boat (Gbb) binds a presynaptic receptor complex composed of the type II BMP receptor kinase Wishful Thinking (Wit) and the type I BMP receptor kinases, Thickveins (Tkv) and Saxophone (Sax) (5,6,8). Through dynein-dependent retrograde trafficking, this complex is transported along the axon and phosphorylates Mother against dpp (Mad), a transcription factor (9). Phospho-Mad (pMad) associates with Medea (Med) and accumulates in the nucleus to bind *BMP-responsive elements* (*BMP-RE*) and to regulate downstream gene expression required for BMP-dependent synaptic functions (8,10,11). The pMad/Med transcription factor activity is postulated to control most BMP-dependent synaptic functions at the NMJ because most of the synaptic defects observed in loss of function mutants for *gbb*, *tkv*, *sax* and *wit* are also present in *Mad* and *Med* mutants, as well as upon overexpression of DNA-binding defective Mad in motor neurons (5,8,11,12).

*To whom correspondence should be addressed. Tel: +1 604 827 5960; Fax: +1 604 822 2316; Email: doug.allan@ubc.ca
Correspondence may also be addressed to Robin Vuilleumier. Email: robvuill@mail.ubc.ca

Despite the critical importance of BMP-dependent transcription in fly motor neurons, only two BMP-activated target genes, *trio* and *twit*, have been confirmed as effectors of NMJ function and maturation. However, overexpression of either of these genes in *wit* mutants only partially rescued the synaptic defects, implicating roles for other unknown BMP targets (13,14). Additionally, it is interesting to note that our current understanding on the role of these BMP-regulated genes in NMJ growth and function is only based on the analysis of null mutant phenotypes. Therefore, the generation of mutants that selectively test the contribution of BMP input on the expression of these target genes would better demonstrate how retrograde BMP signaling regulates synaptic functions.

We recently reported that the pMad/Med complex directly binds *BMP-activating elements (BMP-AEs)* to upregulate BMP target genes in fly motor neurons in the larval ventral nerve cord (VNC) (10). Pioneering studies performed in other *Drosophila* tissues revealed that BMP-dependent activation is also mediated by an indirect derepression mechanism (15,16). In this case, the absence of BMP signaling allows expression of the transcriptional repressor encoded by *brinker* (*brk*), which represses BMP-activated target genes (17–19) (Figure 1A). In the presence of BMP signaling, *brk* transcription is repressed by the direct binding of the pMad/Med complex together with the corepressor Schnurri (Shn) at *BMP-silencer elements* (*BMP-SEs*). Thus, BMP signaling indirectly upregulates target genes in those tissues (20,21). Notably, in addition to *brk*, the *BMP-SE* mediates the direct BMP-dependent repression of numerous genes in other tissues (22–26). In motor neurons, any role for the *BMP-SE* in direct gene repression is unknown.

Here, we use computational DNA motif discovery, *in vivo* reporter assays and genome engineering to identify the downstream gene regulatory program controlled by BMP signaling in motor neurons. We show that BMP signaling upregulates a network of genes, including many with established synaptic functions and/or implicated in neurological disorders. Most of those BMP-upregulated genes harbor conserved *BMP-REs* in their locus, suggesting that these target genes are directly regulated. Surprisingly, we find that *BMP-SE*s operate as activator motifs for neuronal gene expression, as opposed to their strict silencer function in other tissues. Finally, targeted mutation of *BMP-RE* motifs demonstrates the discrete requirement of BMP transcriptional input to the active zone scaffolding gene *bruchpilot (brp)* and to a novel gene, *without maturity (witty)*, in the control of NMJ maturation.

MATERIALS AND METHODS

Fly strains

Flies were reared on standard medium at 25°C, 70% humidity. *UAS-cg14274*-dsRNA (TRIP.JF03191; BL#28763), *UAS-mCherry* (Valium10; BL#35787) *6935-hid* (BL#25679), $Gal4^{221w-}$ (BL#26259), *Df(2L)BSC200* (BL#9627), *Df(2R)BSC408* (BL#24912), *hs-Cre* (BL#851), *OK6-gal4* (BL#64199), *repo-gal4* (BL#7415), brk^{XA}(BL#58792) (17), *tub-PBac* (BL#8283), wit^{A12} and wit^{B11} (BL#5173 and #5174) (5) were obtained from the Bloomington *Drosophila* stock center.

Genotypes by figure

Figure 3A. *w;;Van75,80nlsLacZ,* wit^{A12}*/+. w;;Van65nlsLacZ,* wit^{A12}*/Van65nlsLacZ.* Figure 3B. *w;;Van75,80nlsLacZ,* wit^{A12}*/+.w;;Van65nlsLacZ,* wit^{A12}*/Van65nlsLacZ.w;;Van75,80nlsLacZ,* wit^{A12}*/*wit^{B11}*. w;;Van65nlsLacZ,* wit^{A12}*/Van65nlsLacZ,*wit^{B11}. Figure 3E. *w;;Van75,80nlsLacZ/+.w;;Van65nlsLacZ/Van65nlsLacZ. w;;Van75,80*$^{\Delta mad}$*nlsLacZ/+.w;;Van65*$^{\Delta mad}$*nlsLacZ/ Van65*$^{\Delta mad}$*nlsLacZ.* Figure 3F. *w;;Van75nlsLacZ/+.w;;Van75*$^{SE>AE}$*nlsLacZ/+. w;Van26nlsDsRed/+.w;Van26*$^{AE>SE}$*nlsDsRed/+.* Figure 4. *w;;Van36nlsLacZ/+.w;;Van36* $^{AE>SE}$*nlsLacZ/+.* Figure 5A. *w;Shn::HA/Shn::HA;repo-gal4/UAS-nlsEGFP.* Figure 5B-C. w*;ok6-Gal4,UAS-nlsEGFP;Van75nlsLacZ/+.* w*;ok6-Gal4,UAS-nlsEGFP; UAS-ShnCT/Van75nlsLacZ.w;ok6-Gal4,UAS-EGFPnls;UAS-ShnCT/Van75*$^{SE>AE}$*nlsLacZ.* Figure 5E,F. *yw/Y;Van26nlsDsRed/+.yw,brk*^{XA}*/Y;Van26nlsDsRed/+.* Figure 6B–D. *w;* $brp^{BMP\text{-}SE}$*/Df(2R)BSC408. w;* $brp^{BMP\text{-}SE\Delta mad}$*/Df(2R)BSC408.* Figure 6F,G. *w.w;Ly6Del/Ly6Del. w; R-Ly6AE/R-Ly6AE.w; R-Ly6AE*$^{\Delta mad}$*/R-Ly6AE*$^{\Delta mad}$. Figure 6H,I. *UAS-Dicer2/w; +/Ly6Del;UAS-mCherry/+. UAS-Dicer2/w; +/Ly6Del; elav-Gal4/UAS-dsRNA-witty.*

RNA-seq analysis and enrichment of *BMP-AE* and *BMP-SE* motifs near BMP-regulated genes

For a detailed description of our multi-pipeline RNA-seq analysis, refer to (10). Differential expression between control and *wit* null mutant wandering third instar larval VNCs is represented as $\log_2$ fold change.

To test for enrichment of *BMP-AE* and *BMP-SE* motifs as well as *bcd*-responsive fragments (27) to BMP-responsive genes in the CNS and the embryonic blastoderm, the location of both *BMP-RE* motif types (*BMP-AE* with BLS > 0.6 and *BMP-SE* with BLS > 0.7) and the *bcd*-responsive fragments was mapped with the BMP-responsive genes identified by our RNA-seq and by previous work (28). The number of *BMP-RE* motifs or *bcd*-responsive fragments within 50 kb of the transcriptional start site of a BMP-responsive gene was then counted. Statistical significance of the enrichment was calculated using Pearson's Chi square test for count data in R (function chisq.test) with continuity correction without correcting for multiple testing (http://www.R-project.org/).

GO term over-representation analysis

Analysis of the DE genes in *wit* null mutant ventral nerve cord (VNC) was performed using our previous RNA-seq (10). Gene ontology over-representation analysis of the *wit* DE genes was carried out using PANTHER (http://pantherdb.org/) (29,30) and DAVID (https://david.ncifcrf.gov) (31,32). For PANTHER, the Fisher's exact test and Bonferroni correction for multiple testing was applied. For DAVID, the Benjamini correction was used to determine the *P*-value.

Construction of a neurotransmission gene network

The 453 genes that relate to neurotransmission identified in PANTHER were used to build a neurotransmission gene network in STRING (https://string-db.org/) (33). The meaning of network edges and the active interaction sources were defined as evidence, experiments and databases, respectively. The neurotransmission gene network was then exported into Cytoscape (v3.8.0) and displayed using the yFiles organic layout (34).

DisGeNET analysis of the BMP-upregulated genes

We used DIOPT (https://www.flyrnai.org/diopt) (35) and Ensembl ortholog (36) prediction tools to retrieve the 1086 putative human orthologs of the 637 *Drosophila* BMP-upregulated genes identified in our RNA-seq, using the 'Return only best match' option. We used the DisGeNET application in Cytoscape (v3.8.0) (37–39) to build a disease to gene interaction network, applying the curated source with the strong evidence level to identify human orthologs involved in nervous system diseases. The yFiles radial layout was then used to display the network. We used the MGI Mammalian Phenotype Level 4 2019 in Enrichr (https://amp.pharm.mssm.edu/Enrichr) (40–42) to determine any enrichments of the 1086 putative human orthologs for neuronal and synaptic mice phenotypes.

BMP-SE identification and prioritization

Using merMer (http://www.insilicolabs.com/cgi-bin/style.cgi) (43), we identified 385 occurrences matching the consensus *BMP-SE* motif (*GRCGNCN$_5$GTCTG*) in the *Drosophila melanogaster* genome. Of these, we selected 261 *BMP-SE* motifs located in intronic, UTR and intergenic regions and filtered them by the controlled Branch Length Score (BLS) to motif confidence to evaluate phylogenetic conservation over 12 *Drosophila* species with the assistance of the Stark group. A BLS confidence score based on the relative conservation of the *BMP-SE* motif and control motifs was assigned (Supplementary Figure S3). To generate reporter constructs for *in vivo* testing of enhancer activity, we first selected all 20 *BMP-SE*s with a motif confidence $\geq$0.9 directly located within 12 kb of a *wit*-responsive gene. To obtain more instances to test, we also selected 14 additional *BMP-SE*s: (i) with a motif confidence $\geq$0.8 that locates within 12 kb of a strong *wit*-responsive gene ($\log_2$(FC) $\geq$ 0.6), (ii) with a motif confidence of 0.8 that is 'paired' with another *BMP-SE* of motif confidence $\geq$0.9 within 12 kb of the same annotated gene locus, (iii) with a motif confidence $\geq$0.8 located within 12 kb of a BMP-repressed gene or (iv) with a motif confidence $\geq$0.8 located within 12 kb of a BMP-upregulated gene of interest. The initial computational analysis used the Release 3 of the *D. melanogaster* reference genome (Dm3) (44). To calculate the proximity of *BMP-SE*, *BMP-AE* and *bcd* genomic fragment (27) to BMP-regulated genes, the coordinates of the motifs were later converted to Release 6 (Dm6) (45). *Wit*-responsiveness of neuronally expressed genes was determined using our previous RNA-seq (10).

Drosophila DNA constructs and transgenic flies

To generate reporter constructs, we used the same approach as described previously (10) using primers reported in Supplementary Table S1. Mutagenesis was carried out using the Q5 site-directed mutagenesis kit (NEB) or by SOE-PCR using primers designed to introduce the specific mutations. All constructs were verified by sequencing.

For fly transgenesis, reporter constructs were inserted via PhiC31 integrase-mediated site-specific integration at insertion site *attP40* (25C6) on chromosome 2 or *attP2* (68A4) on chromosome 3 by Genetics Services Inc. (MA, USA) and Rainbow Transgenics Flies Inc. (CA, USA).

Genome engineering by CRISPR and ends-out targeting

The endogenously tagged HA::Brk and Shn::HA alleles were generated using CRISPR/Cas9 genome engineering in combination with PhiC31integrase-mediated site-specific recombination. Briefly, the coding sequence and parts of the 5'UTR and 3'UTR of *brk* and *shn* were removed using Cas9, guide RNAs (gRNAs) and homology arms (HAs) (*brk*: 5': chrX: 7 307 101–7 308 108; 3': chrX: 7 310 681–7 311 658; *shn*: 5': chr2R: 11 206 075–11 207 317; 3': chr2R: 11 216 395–11 217 557) flanking the guide RNAs recognition sites. The gRNAs and HAs were, respectively, cloned into the pCFD4 and pHD-dsRed-attP plasmid (Addgene) (46). Plasmids were co-injected into *nos-Cas9* embryos, and modified flies were identified in the progeny using the 3xP3::dsRed marker, which was subsequently removed by Cre recombinase. The deleted regions were then reconstituted by standard PhiC31/attB transgenesis using the RIVwhite_3xHA::brk and RIVwhite_Shn::3xHA plasmids. The RIVwhite plasmid (47) including 3xHA::brk contains the deleted *brk* exon and the sequence encoding three copies of the HA tag inserted directly downstream of the start codon. The RIVwhite_Shn::3xHA plasmid contains the full-length coding cDNA with the deleted part of the 3'UTR and the sequence encoding three copies of the HA tag prior to the stop codon. Transformants were identified by the presence of the *w* + marker, which was then excised using Cre recombinase.

To mutate the *BMP-SE* of the *brp* locus, we used the scarless gene editing procedure described in https://flycrispr.org/scarless-gene-editing/. Briefly, overlapping extension PCR was used to insert the two homology arms (5': chr2R: 9 512 865–9 513 874; 3': chr2R: 9 513 972–9 515 364) that carry either a mutated or a wild-type *BMP-SE* motif and the 3xP3::eGFP pBac transposon cassette into the pJet 1.2 (ThermoFisher) donor vector. The 2 guide RNA sites surrounding the *BMP-SE* motif (sequence reported in Supplementary Table S1) were identified using the CRISPR Optimal Target Finder (48) and subsequently cloned into the sgRNA (pU6-BbsI-chiRNA) vector (Addgene). To avoid multiple CRISPR-mediated excision events, both PAM sequences were mutated. To account for possible off-target effects of CRISPR, a donor construct with a wild-type *BMP-SE* and mutated PAM sequences was used as control. Mutant and wild-type donor vectors were injected into *nos-Cas9* fly embryos, along with the two corresponding sgRNA vectors (Rainbow Transgenics Flies Inc., CA, USA). EGFP

screening in progeny of injected flies was performed using a Leica MZ10 F Stereo Microscope. Removal of the 3xP3::eGFP transposon cassette in transformants was carried out using piggyBac transposase. After confirmation by sequencing, this procedure yielded two independent lines for the mutant *BMP-SE* and one line for the wild-type *BMP-SE*.

To perform genomic engineering of the Ly6 gene cluster, we followed the procedure described in (49–51). In summary, the PCR amplified 5' (chr2L: 8,318,763–8,323,873) and 3' (chr2L: 8,338,698–8,342,585) homologous regions flanking the Ly6 genes cluster were cloned into the targeting pGX-attP-WN vector using the restriction sites NotI/Acc65I and BglII/XhoI, respectively. Following P-element mediated transgenesis (Genetics Services Inc., MA, USA), the targeting DNA was excised and linearized using Flippase and I-SceI. Targeted 'knock out' events were selected using the dual selection marker W::Neo ([G418] in food = 0.17 mg/ml). A total of 400 000 progeny were screened, yielding 110 potential candidates of which two were found to be correctly targeted events, as confirmed by sequencing. The W::Neo marker was then excised using Cre recombinase resulting in the final *Ly6Del* mutant allele, in which 14,825 bp of the Ly6 genes cluster is replaced with an *attP* and *loxP* site. To restore wild-type and mutated genomic fragments, we integrated sequences of the Ly6 genes cluster into the *attP* site of *Ly6Del*; the genomic fragment was PCR-amplified and inserted into the pGE-attB^{GMR} vector using the NotI/Acc65I restriction sites. Mutagenesis of the four *BMP-AE* motifs was carried out by SOE-PCR using primers designed to introduce the specific mutations. Partial deletions of the *Ly6* gene cluster were performed using the restriction site NotI/SpeI and AscI/Acc65I. Mutagenesis was carried out by SOE-PCR using primers designed to introduce the specific mutations. All constructs were verified by sequencing. These constructs were inserted via PhiC31 integrase-mediated site-specific integration into *Ly6Del (*Rainbow Transgenics Flies Inc. CA, USA). The *w* + marker from the obtained transformants was excised using Cre, resulting in flies that harbor a wild-type or mutated Ly6 genes cluster flanked by an *attR* and a *loxP* site.

Electrophoretic mobility shift assay (EMSA)

Electrophoretic mobility shift assays (EMSA) were carried out as in (10). The sequence of the probes are indicated in Supplementary Table S1.

Dissection, immunofluorescence and microscopy

Standard procedures were used for immunostaining *Drosophila* wandering third instar VNCs and NMJ4s. To immunostain GluRIIA at NMJ4, Bouin's solution was used as fixative for 5 min at room temperature. For NMJ dissections, variation in developmental stage between experimental groups was minimized by transferring first instar larvae to fresh vials at a density of 80 larvae/vial until the desired stage. The synapse located at muscle 4 within abdominal segment 2–5 was selected for analysis. Primary antibodies were mouse anti-Brp (1:20; nc82), mouse anti-GluRIIA (1:50; 8B4D2) and mouse anti-Dlg (1:50 4F3) (Developmental Studies Hybridoma Bank, University of Iowa, USA); chicken anti-βgal (1:1000; ab9361); rabbit anti-pSmad1/5 (1:100; 41D10; Cell signaling Technology), rat anti-HA (1:100; 3F10; Roche). Secondary antibodies were donkey anti-Mouse, anti-Chicken, anti-Rabbit conjugated to FITC, DyLight 488, Cy3, Cy5 and Alexa 647 (1:500–1:1000; Jackson ImmunoResearch). Images of experimental groups were captured with the same settings with an Olympus FV1000 and Zeiss 880 confocal microscopes.

Quantification of immunofluorescence for reporter expression in the VNC and molecular markers at NMJ4

Bitplane:Imaris v9.2.1 software was used to quantitate reporter activity in nuclei of the VNC and fluorescence intensity of molecular markers at NMJ4. Nuclear reporter activity quantification was carried out as described previously (10). For intensity measurements at NMJ4 (Brp: abdominal segments 2–5, GluRIIA/Dlg: 2–3), the total region of synaptic boutons (HRP staining) was defined using the 'Surfaces' tool to select the appropriate NMJ. For each experimental group, an intensity threshold was then selected to ensure the created surface encompasses the entirety of the molecular marker and HRP-stained region. The 'Cut' function was used to remove irrelevant structures. To quantify Brp punctae, the surface was then converted to a binary mask, and the 'Spots' mode function was used to select the punctae. An estimated XY diameter was calculated by measuring the diameter of select punctae with the 'Line' measurement function. For each experimental group, an appropriate threshold was selected to ensure the maximum number of punctae were captured while minimizing false positives. Accuracy of the 'Spots' function was validated by manually calculating the volume of selected punctae by measuring its length and radius using the 'Line' function and approximating its volume as a bicone. Finally, calculated spots were filtered for those which are only found within the region defined by the HRP-stained binary mask surface. The total volume and intensity of Brp punctae, and also HRP staining, were automatically calculated and extracted. For the quantification of GluRIIA and Dlg immunofluorescence at NMJ4, a similar procedure to that for Brp was used, except that the total intensity of these molecular markers was calculated using the 'Surface' mode function and no HRP-stained binary mask was used.

Statistical analysis

Statistical analysis was performed using the online tools at https://www.statskingdom.com/, http://ccb-compute2.cs.uni-saarland.de/wtest/ (52) and https://astatsa.com/KruskalWallisTest/. To determine whether sample populations were normally distributed, the Shapiro–Wilk test was used. All comparisons were performed using the Student's *t*-test, one-way ANOVA or the nonparametric Wilcoxon rank-sum and Kruskal–Wallis rank sum tests. For RNA-seq, the Wald test was used and the *P*-value was adjusted with the Benjamini–Hochberg FDR method. Differences between genotypes were considered significant when $P < 0.05$. Data are represented as

mean ± standard error of the mean (SEM) and graphing was carried out using MS Excel.

RESULTS

Identification of a neuronal BMP gene regulatory network

To identify target genes that mediate the downstream function of BMP-dependent transcription in motor neurons, we examined differentially expressed genes in *wit* null wandering third instar larvae (10) (Figure 1B). Among the 9868 genes expressed in the VNC, 1201 genes (12.2%) were significantly differentially expressed (DE); 637 (6.5%) were downregulated, and 564 (5.7%) genes were upregulated (Figure 1C and Supplementary Table S2). To reveal whether DE genes were enriched within functionally related gene networks, GO term over-representation analysis using the functional annotation tools, PANTHER (29,30) and DAVID (31,32), was applied to DE genes. Of the 564 genes upregulated in *wit* nulls (BMP-downregulated), no biological processes were over-represented. In contrast, of the 637 genes downregulated in *wit* nulls (BMP-upregulated), PANTHER identified 16 over-represented biological processes, of which six were related to neurotransmission, with the others also pertinent to the reported *wit* NMJ phenotype, including 'cell-cell adhesion via plasma membrane adhesion molecules' and 'synapse organization' (Figure 1D). Genes over-represented by Cellular Component were mostly localized to the synapse, and those over-represented by Molecular Function were mostly related to amino acid transport and ion transport, as well as neuropeptide/neurohormone signaling. Similar findings were obtained using DAVID (Supplementary Figure S1A). Thus, because BMP activity is mostly restricted to motor neurons in the VNC, these data indicate that retrograde BMP signaling upregulates a large number of genes that coordinately regulate synaptic growth and neurotransmission in motor neurons (5–7).

Persistent retrograde BMP signaling and downstream transcription is required to maintain neurotransmission and allow for plasticity throughout larval growth, but the downstream target genes are largely unknown (7,12). Using our data to identify candidate genes, we focused on the network of neurotransmission genes (NT) that is over-represented for BMP-activated genes. The six over-represented GO term categories that relate to neurotransmission comprise a total of 453 genes, of which 110 are BMP-responsive (24.3% of genes in the network), including 86 BMP-upregulated (19%) and 24 BMP-downregulated (5.3%) genes (Figure 1D and E; Supplementary Figure S2). Within this NT network, we found four major interaction clusters (I–IV) that contain 38 BMP-upregulated genes encoding key regulators of neurotransmission, neurotransmitter transporters (*VGlut, Eaat1*), ion channels (*nAChRα1, mGluR, 5-HT1A, eag*), modulators of ion channels (*Grip, Slob*), active zone organization and synaptic vesicle fusion (*Brp, Syx1A, Syt1, nSyb, Comt, Snap24, Cpx, Tomosyn*) and vesicle recycling (*rab3, StnB*) (Figure 1E and Supplementary Figure S2). We further subdivided the 110 *wit*-responsive genes within this broad neurotransmission category into five groups of related gene function: (i) NT synthesis and transport, (ii) cell adhesion and cytoskeleton, (iii) signaling, (iv) transcription and RNA, and (v) metabolism and others (Figure 1E and F). We found that the majority of the *wit*-responsive gene groups were BMP-upregulated, except for the 'metabolism and others' group, which shows a 1:1 ratio (Figure 1F). Thus, BMP signaling transcriptionally upregulates a gene network encoding functionally interacting components of NMJ neurotransmission.

To lift these findings over to mammalian phenotypes and human disease, we first identified the highest scoring human orthologs (1086 genes) of the 637 BMP-upregulated genes, using DIOPT (35). Using EnrichR (40–42) with mammalian phenotypes in MGI, we observed significant enrichments for neuronal and synaptic phenotypes, particularly related to neurotransmission and synaptic plasticity (Supplementary Figure S1B). Second, we examined disease associations for the 1086 human orthologs. Using DisGeNET (37–39) with stringent settings, we found that 85 human orthologs were associated with 14 diseases including intellectual disability, spastic paraplegia, Parkinson disease and Charcot-Marie-Tooth disease (Figure 1G and Supplementary Table S3). Altogether, we conclude that retrograde BMP signaling upregulates neurological disease-relevant genes to promote synaptic function.

BMP-AE and *BMP-SE* motifs mediate BMP-dependent upregulation of neuronal gene expression

Having identified a BMP-regulated synaptic gene network, we then assessed the proportion of these genes that are directly regulated by BMP signaling in motor neurons. Because the CNS displays great cell-subtype diversity with a relatively low number of motor neurons that makes genomics methods to identify pMad bound regions challenging, we opted for a computational approach to test for enrichment of *BMP-AE* (*GGCGCCAN$_4$GNCV*) and *BMP-SE* (*GRCGNCN$_5$GTCTG*) motifs, for which the GGCGCC/GRCGNC sequences are bound by pMad and the GNCV/GTCT sequences are bound by Med (21,53). Previously, we found that the BLS to motif confidence method (54) efficiently identified functional *BMP-AE* motifs that upregulate expression of nearby genes in motor neurons (10). *BMP-SE* motifs are established BMP-dependent silencers of gene expression during embryogenesis, growth and patterning of larval imaginal discs, yet their function remained unexamined in neurons.

To determine if the BLS method can predict functional *BMP-SEs*, we filtered the 261 strict *BMP-SE* motifs found in the noncoding *Drosophila* genome using BLS (Supplementary Figure S3) and identified 154 conserved *BMP-SE*s based on the strict consensus sequence (*GRCGNCN$_5$GTCTG*). These were used to calculate enrichment near BMP-regulated genes found in transcriptomic datasets reporting differential gene expression upon ubiquitous BMP-activation in the embryonic blastoderm (28). Confirming expectations, *BMP-SE* motifs were significantly enriched near BMP-downregulated genes, and *BMP-AE* motifs near BMP-upregulated genes. A control set of Bicoid (Bcd)-responsive genomic fragments showed no enrichment (Figure 2A). This confirmed that the BLS approach accurately predicts functional instances of these two motifs genome-wide.

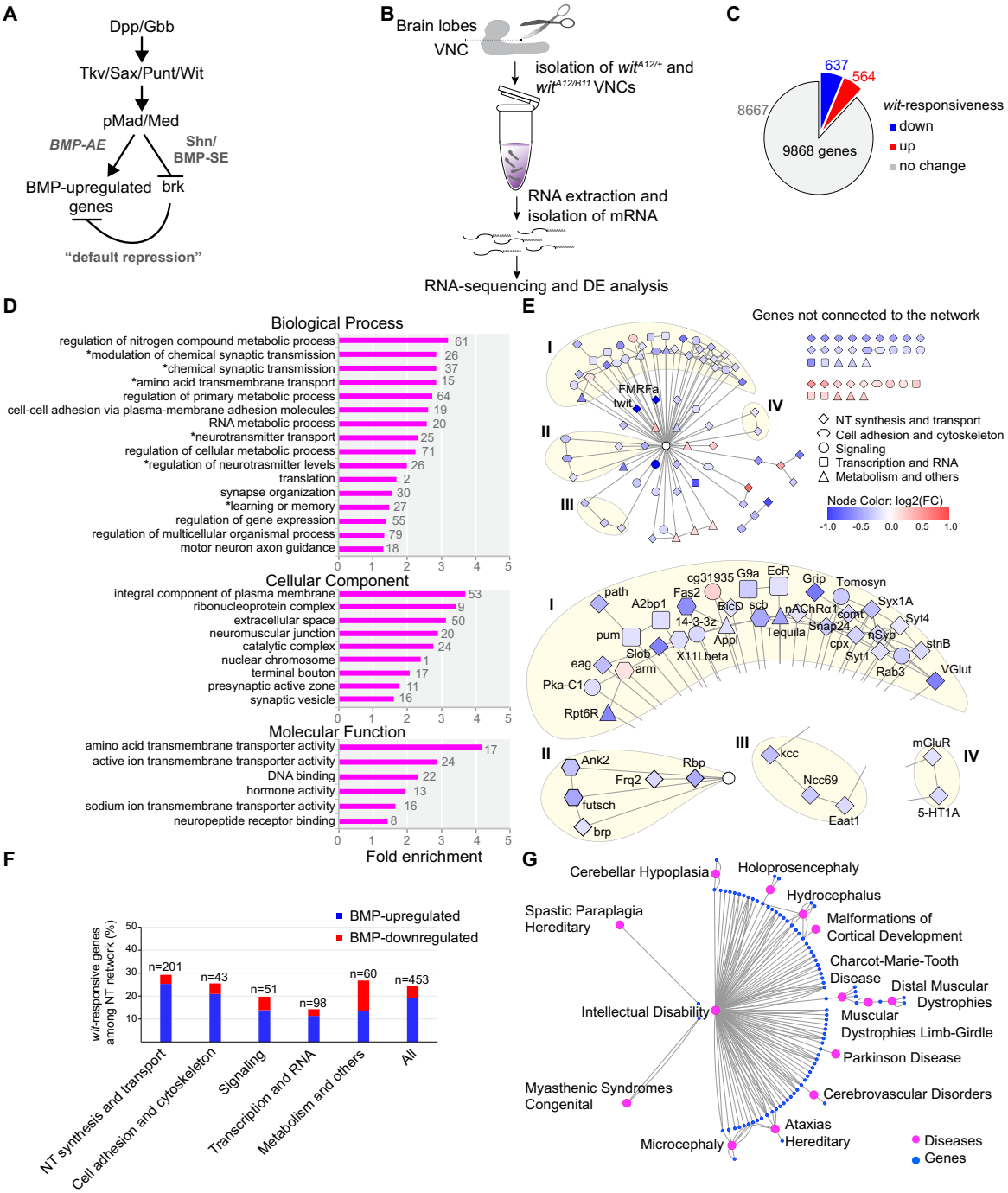

Figure 1. (**A**) Schematic of the canonical BMP signaling pathway in *Drosophila*, noting the direct activation arm via *BMP-AE* and the default repression arm via *BMP-SE* to repress the *brk* transcriptional repressor. (**B**) Schematic of the RNA-seq experiment to examine differential gene expression (DE) between control and *wit* null VNCs, with the brain lobes removed. (**C**) The number of genes that were downregulated (blue), upregulated (red) or not affected (gray) in *wit* nulls. (**D**) PANTHER Gene Ontology (GO) over-representation analysis for the 637 genes upregulated by BMP signaling. The number of over-represented genes within each term are provided next to each bar. The fold enrichment is the $-\log_{10}$(*P*-value). (**E**) A neurotransmission network of 453 genes is shown, with blue and red nodes indicating genes that are BMP-upregulated and downregulated, respectively. The color intensity of the nodes defines the log2 (fold change) of DE. All *wit*-unresponsive genes are indicated as a single central white node. Genes are classified based on their function as shown beside the network. Four major interaction clusters are shown (I–IV). (**F**) Bar graph showing the proportion of *wit*-responsive genes in each functional category shown in panel (E). (**G**) Disease to gene interaction network for the 1086 putative human orthologs using DisGeNET analysis.

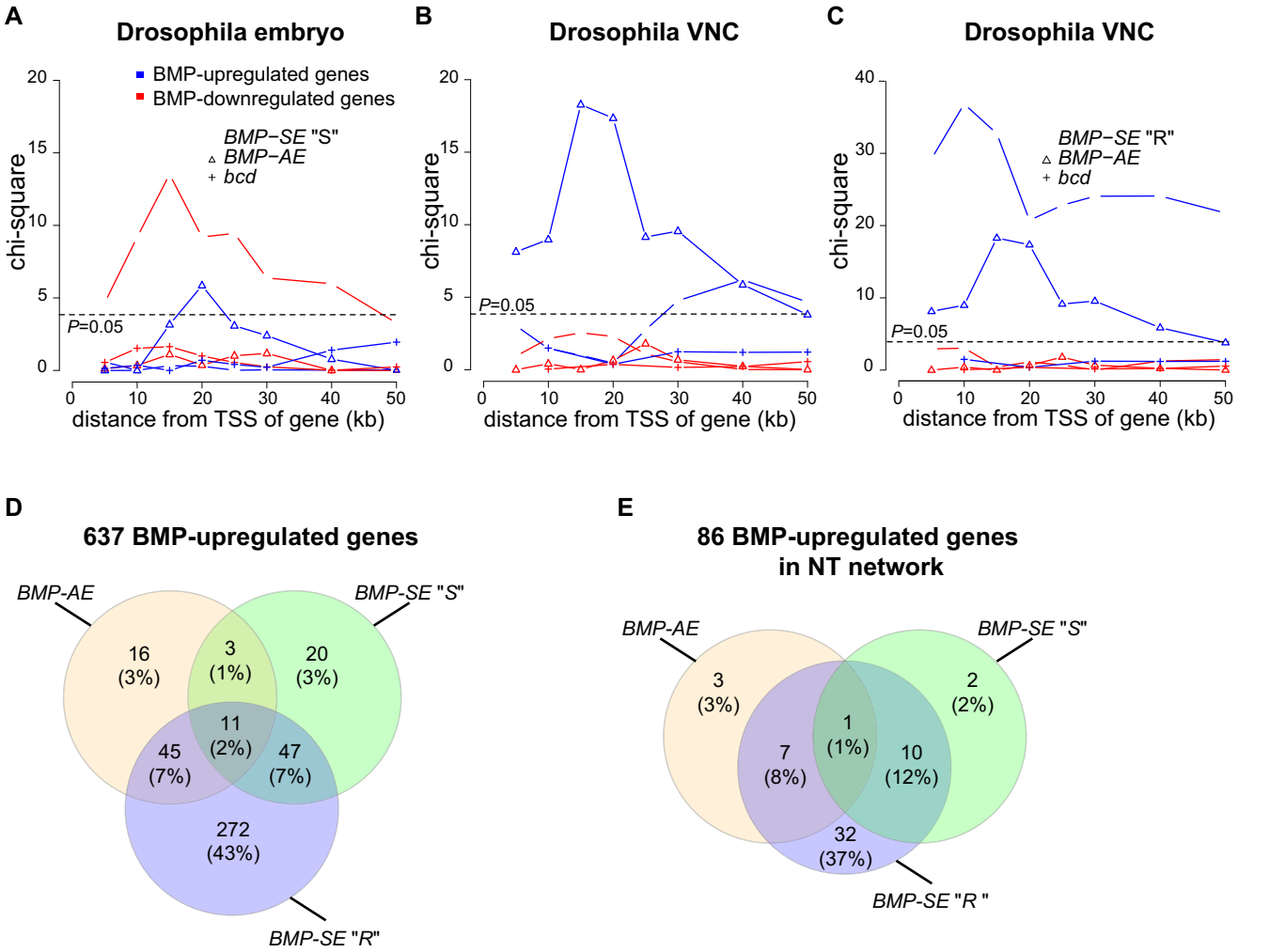

Figure 2. (**A**–**C**) Chi-square calculation of enrichment of *BMP-AE*s and *bcd*-responsive genomic fragments as well as strict (A,B) and relaxed (C) *BMP-SE* motifs (strict *BMP-SE* denoted 'S', relaxed *BMP-SE* denoted 'R') to BMP-responsive genes in (A) published RNA-seq datasets from the embryonic blastoderm and (**B,C**) larval VNCs. All motifs that exceed the threshold *P*-value of 0.05 are considered significantly enriched. The *x*-axis indicates incremental distance (in kb) of the motifs from the transcriptional start site (TSS) of expressed genes. Strict *BMP-SE* motifs are excluded to calculate enrichment of relaxed *BMP-SE* motifs. (**D**–**E**) Venn diagrams showing the number of all neuronal BMP-upregulated genes (D) and specifically those in the neurotransmission (NT) network (E) that contain a *BMP-AE* and/or *BMP-SE* motifs within 50 kb of their TSS.

We performed the same analysis using our *wit* null VNC RNA-seq datasets (10). Extending our previous findings, we found that conserved *BMP-AE*s were significantly enriched to BMP-upregulated genes but not to BMP-downregulated genes (Figure 2B). However, unexpectedly, *BMP-SE*s were also significantly enriched near BMP-upregulated genes and not to BMP-downregulated genes (Figure 2B). A parsimonious explanation for this observation would hold that the *BMP-SE* may operate as an atypical activator motif in motor neurons, in contrast to its strict repressive function in other tissues.

Recruitment of the pMad/Med complex and Shn to the *BMP-SE* requires the strict consensus sequence of Med-recruiting nucleotides at positions 12, 14 and 15 for repressor activity (21). In contrast, positions 13 and 16 of the *BMP-SE* motif display less strict consensus sequence requirements (55). Therefore, we tested whether a relaxed *BMP-SE* motif (*GRCGNCN*$_5$*GTCTG* to *GNCGNCN*$_5$*GNCT*) would increase enrichment near BMP-upregulated genes. Confirming this prediction, we found that relaxing the *BMP-SE* motif increased the enrichment of *BMP-SE* at BMP-upregulated genes, but not at BMP-downregulated genes, supporting the hypothesis that *BMP-SE* motifs mediate BMP-upregulation of numerous neuronal target genes (Figure 2C).

These data provide evidence that both *BMP-RE*s mediate direct BMP-dependent upregulation of neuronal gene expression. Indeed, 22% (142/637) of the BMP-upregulated genes harbor a conserved *BMP-AE* and/or strict *BMP-SE* within 50 kb of their transcription start site (TSS) (Figure 2D). Moreover, when considering the more relaxed *BMP-SE* motif, we found that 65% (414/637) of the BMP-upregulated genes harbor a conserved *BMP-RE* within 50 kb of their TSS (Figure 2D). A similar 64% (55/86) was observed when only the BMP-upregulated genes of the NT network were considered, indicating that neurotransmis-

sion at the NMJ is controlled by a large number of genes that are likely directly upregulated by BMP-signaling (Figure 2E and Supplementary Table S4).

BMP-SE upregulates reporter gene expression in motor neurons

To obtain functional evidence that *BMP-SE* motifs operate as transcriptional activators in motor neurons, we selected 34 conserved *BMP-SEs* for *in vivo* testing, based on their close proximity to *wit*-responsive genes. Genomic fragments containing those 34 *BMP-SE*s were cloned into nuclear *lacZ* reporter constructs to test their reporter activity in larval VNCs. We found that 24 (70.6%) of these DNA fragments drove reporter expression in the VNC, and that 16 (47.1%) were active in pMad positive neurons (Figure 3A and Supplementary Table S1). To assess whether these 34 genomic fragments are BMP-regulated, we tested reporter expression in *wit* nulls. We found that 11 of the 16 reporters active in pMad positive neurons (69%) displayed a loss of expression in *wit* mutants, and that only 1 out of the 34 reporters (2.9%) exhibited upregulation (Figure 3B, Supplementary Figure S4A and Table S5). This further supported our hypothesis that the *BMP-SE* motif primarily mediates BMP-dependent activation in the VNC. We next tested whether the activity of these genomic fragments is controlled by the embedded *BMP-SE* motif. To this end, we selected three *BMP-SE*s, based on strong *wit*-responsiveness of their corresponding genomic fragments and examined the recruitment of pMad/Med complexes at those motifs by EMSA. Lysates of Schneider 2 cells (S2) transfected with Mad, Med and a constitutively activated Tkv (Tkv^{QD}) were tested for their capacity to band shift IRDye700 tagged probes containing those *BMP-SE*s (Figure 3C and D). We found that the pMad/Med complex shifted each labeled probe, indicating its binding to the *BMP-SE* motifs. These interactions were sequence specific, since all band shifts were not observed when labeled mutated probes (ΔMad), carrying substitution mutations at the pMad binding, were tested (Figure 3D). Interestingly, we also observed two band shifts, with both the labeled wild-type and mutant probes with lysates of non-transfected and transfected S2 cells. This suggests that additional unknown proteins, found in S2 cells, bind and shift these probes independently of BMP-signaling and the sequence of the *BMP-SE* motif. Thus, we interpret these band shifts as non-specific because they do not represent pMad/Med complex binding at the *BMP-SE* motif. We also observed that a number of these non-specific bands were eliminated upon pMad/Med complex probes binding, which we presume is due to higher affinity of the pMad/Med complex for the wild-type probe than the unknown proteins. These observations were also confirmed in EMSA using unlabeled wild-type and ΔMad-mutated probe competitors (Supplementary Figure S4B).

To obtain *in vivo* evidence that the *BMP-SE* motifs mediate BMP-activation, we mutated the *BMP-SE*s within 5 *wit*-responsive genomic fragments. These *BMP-SE*s were selected because of their significant *wit*-dependent loss of reporter expression (*Van61*, *Van65, Van75, Van80*) or gain of reporter expression (*Van74*). We found that three out of these four BMP-activated genomic fragments displayed a loss of reporter expression due to *BMP-SE* mutation (Figure 3E and Supplementary Figure S4C). In contrast, mutation of the *BMP-SE* within *Van74* did not lead to any change, suggesting that the increase of expression for this reporter in *wit* nulls is not mediated by this motif (Supplementary Figure S4C). Altogether, these data provide functional *in vivo* evidence that the *BMP-SE* mediates BMP-dependent gene upregulation in motor neurons.

The *BMP-SE* displays tissue-specific dichotomous function

Our finding that *BMP-SE* motifs operate akin to the function of *BMP-AE* motifs in the VNC led us to test whether *BMP-SE* and *BMP-AE* sequences are functionally interchangeable in motor neurons. To this end, we converted the *BMP-SE* of the *Van75* reporter into a *BMP-AE* ($Van75^{SE>AE}$), by replacing the thymine at position 15 with a guanine (Figure 3C). Second, we converted the *BMP-AE* of the *Van26* reporter into a *BMP-SE* ($Van26^{AE>SE}$), by replacing the guanine at position 15 with a thymine (Figure 3C). The *BMP-AE* within the *Van26* reporter was previously shown to be essential for its neuronal activity (10). These modifications did not change reporter activity of either genomic fragment (Figure 3F), suggesting that *BMP-SE* and *BMP-AE* motifs are interchangeable gene activators in neurons. However, it is also possible that DNA motifs embedded in sequences adjacent to the *BMP-SE* are responsible for its unique gene activation output in motor neurons. To rule this possibility out, we performed a *BMP-AE* to *BMP-SE* conversion in the *wit*-responsive *Van36* fragment (Figure 4A). This fragment displays BMP-responsiveness in both the wing imaginal disc and in neurons of the VNC (Figure 4B and C) (10,53). In line with our prediction, the $Van36^{AE>SE}$ reporter showed a total loss of expression in the wing disc but maintained wild-type reporter expression in motor neurons (Figure 4B and C). Taken together, these data strongly suggest that the activator function of the *BMP-SE* in motor neurons is independent of additional regulatory motifs in the genomic fragment.

Interestingly, we noted that the *Van36* reporter is also expressed in many glial cells of the VNC, and that this pattern was lost when the *BMP-AE* was mutated into a *BMP-SE* (Figure 4C). Since a role for BMP signaling in gene regulation in glia of the VNC is unknown at this time, it remains unclear whether this observation is artifactual, or due to a BMP-dependent silencing function of the *BMP-SE* in glia.

Absence of the Shn de-repression path for *BMP-SE* mediated activation in motor neurons

Next, we tested for any contribution of Shn to *BMP-SE* function in motor neurons. By both RNA-seq and examination of the expression of a functional C-terminal, HA-tagged allele of *shn* (*shn::HA*), we found that *shn* is indeed expressed in the VNC. By RNA-seq, we did observe a modest but significant downregulation of *shn* in *wit* nulls (Supplementary Figure S5A). However, upon analysis of Shn::HA expression, we found it to be selectively absent from most pMad-positive neurons (91.7% ± 0.9; $n = 4$ VNCs) (Figure 5A) but robustly expressed in other cells.

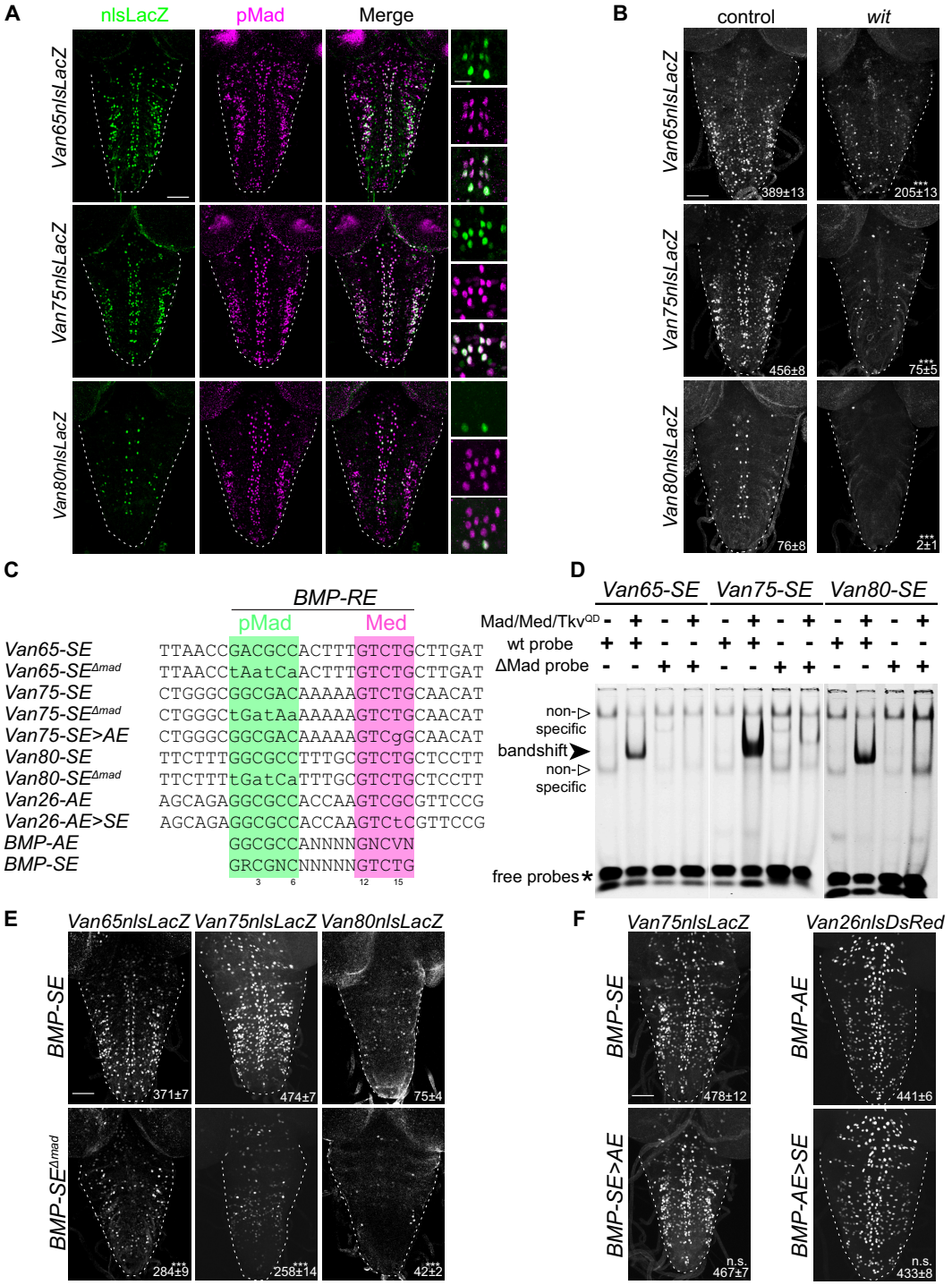

Figure 3. (**A**) Reporter activity (anti-nuclear β-gal immunoreactivity; green), from three genomic fragments containing conserved *BMP-SE*, is localized primarily in motor neurons as revealed by pMad co-staining (magenta). (**B**) Reporter activity of these three genomic fragments is reduced in *wit* nulls. The mean ± SEM number of nuclei per VNC expressing the reporter is indicated (inset). (**C**) Sequences of the consensus, wildtype and mutant *BMP-SE* and *BMP-AE* motifs, examined in the other panels, noting the position number of specific nucleotides in the motif, below. The sequences shown in green and purple are predicted to be bound by pMad and Med as previously shown. (**D**) EMSA for three IRDye700-labeled *BMP-SE* wild-type and mutated (ΔMad) sequences with lysates from S2 cells transfected with the indicated plasmids. A strong band shift for each labeled wild-type probe was only obtained in lanes loaded with S2 cell lysate transfected with Mad, Med and Tkv^{QD} (MMT). The labeled mutated probes did not generate a band shift under the same conditions. Two weak band shifts that we consider non-specific with regard to Smad binding were also obtained for each probe regardless of the absence or presence of MMT or wild-type and mutated probes. (**E**) Reporter activity driven from three *wit*-responsive genomic fragments in which the *BMP-SE* is either wild-type or mutated (ΔMad) at the pMad binding site indicated in panel (C). Reporter activity of mutated genomic fragments was reduced. (**F**) Reporter activity (anti-nuclear β-gal immunoreactivity or DsRed expression) driven from two *wit*-responsive genomic fragments after motif conversion as indicated in panel (C). These mutations did not disrupt reporter activity. ***$P < 0.001$; n.s. not significant (two-sided unequal variance Student's *t*-test) with $n = 5$–9 VNCs per genotype. Scale bars of panels A,B,E,F: 50 μm; A, inset: 10 μm.

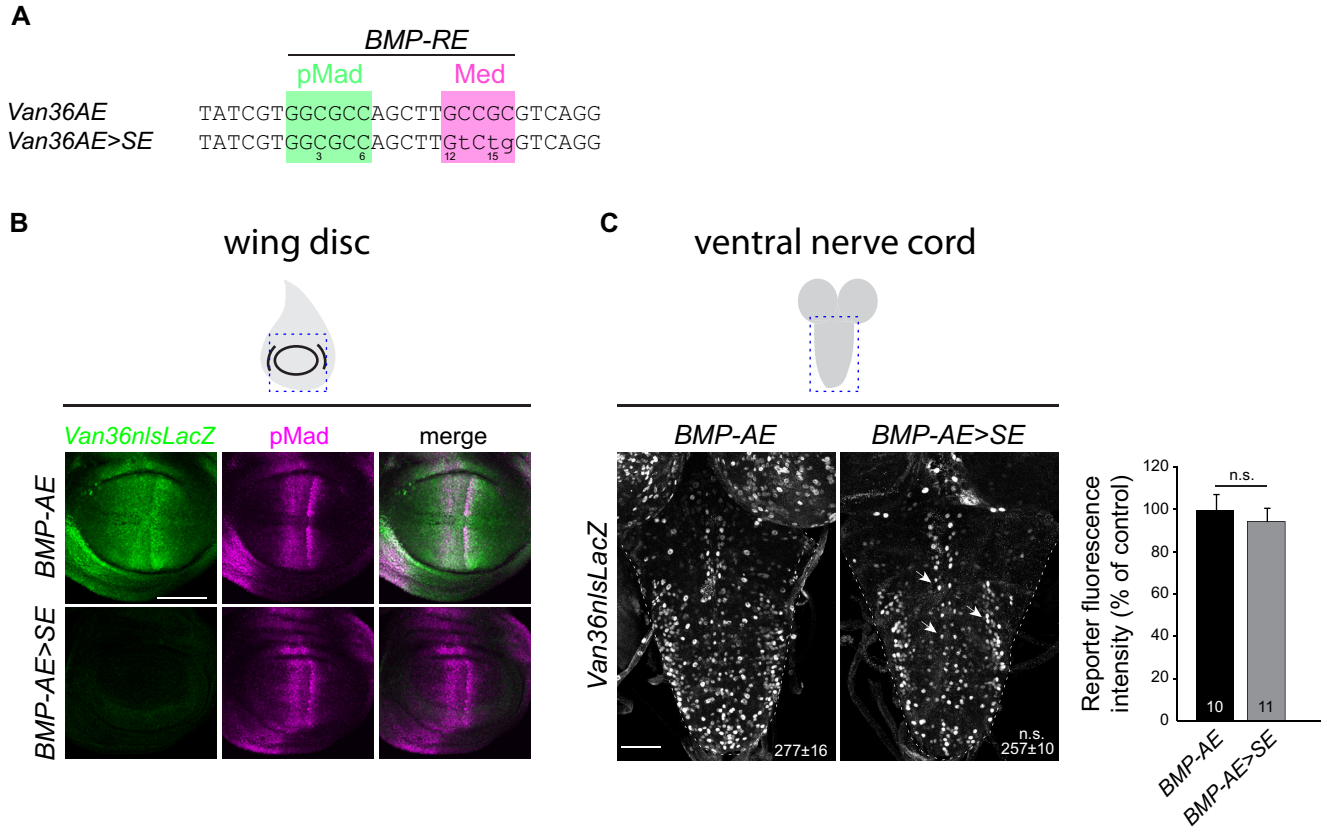

Figure 4. (**A**) Sequences of the wild-type and converted *BMP-AE* examined in panels (B,C). (**B,C**) Comparison of reporter activity (anti-nuclear β-gal immunoreactivity) in the wing disc and VNC, driven from a *wit*-responsive genomic fragment containing either a *BMP-AE*, or a *BMP-AE* > *SE* conversion. (B) In the wing disc, wild-type reporter expression (green) mirrored BMP signaling activity as revealed by anti-pMad immunolabeling (magenta). Activity of the converted *BMP-AE* > *SE* reporter was strongly downregulated. (**C**) In the VNC, motor neuron expression (white arrows) of the *BMP-AE* > *SE* reporter remained unaffected. The mean ± SEM number of motor neuron nuclei per VNC expressing the reporter is indicated (inset). n.s., not significant (two-sided unequal variance Student's *t*-test) with $n = 10$–11 VNCs per genotype. Scale bars of panels (B,C): 50 μm.

This raises the possibility that the absence of Shn in most motor neurons may account for the specific *BMP-SE* activator function in these cells. To test this hypothesis, we misexpressed a subfragment of Shn (ShnCT) in motor neurons, which recapitulates Shn repressive activity (21). In this context, we compared reporter activity of the wild-type *Van75* reporter, which contains a wild-type *BMP-SE*, with a converted *Van75* reporter in which the *BMP-SE* was converted to a *BMP-AE* (*Van75*$^{SE>AE}$). We reasoned that if the *BMP-SE* activator function depends on the absence of Shn in motor neurons, then the wild-type *Van75* reporter would be repressed, whereas the *Van75*$^{SE>AE}$ reporter would not be affected, based on the requirement of Shn activity upon the strict *BMP-SE* consensus sequence. In confirmation of our hypothesis, we observed a 70% loss of reporter activity of wildtype *Van75* compared to a 20% loss of the converted *Van75*$^{SE>AE}$ reporter (Figure 5B and C). The incomplete loss of reporter activity following ShnCT misexpression likely reflects both the lack of BMP responsiveness of the reporter in a subset of VNC cells (see Figure 3B and E) and the low GAL4 expression in certain motor neurons. Alternatively, we cannot rule out the possibility that an additional unknown cofactor that assists in Shn recruitment to the activated Smad complex at the *BMP-SE* is absent in some motor neurons. These data suggest that the absence of Shn in most motor neurons is a prerequisite for the activator function of the *BMP-SE* embedded in the *Van75* reporter.

We then focused on *brk*, a repressor of BMP-activated target genes in many tissues that is repressed by BMP signaling and Shn (Figure 1A). In the VNC, we observed a lack of differential expression for *brk* in *wit* nulls (Figure 5D). This lack of BMP-dependent expression was confirmed by examining expression of a functional endogenously HA-tagged *brk* allele that faithfully recapitulates its expression in the wing disc (Supplementary Figure S5B and C). Next, we explored the possibility that low levels of Brk in motor neurons, not detectable by immunohistochemistry, may still be sufficient to repress potential *BMP-AE*s to control for optimal expression of BMP-upregulated genes. To this end, we analyzed expression of *Van26*$^{BMP\text{-}AE}$, a sensitive BMP-dependent reporter expressed in many motor neurons, in *brk*^{XA}strong hypomorphs. We found no change in the activity of *Van26*$^{BMP\text{-}AE}$ in motor neurons (Figure 5E and F), suggesting that *brk* does not repress *BMP-AE*s.

We conclude that downstream BMP signaling transcriptional outcomes in motor neurons do not operate in the context of the de-repression path involving *brk* and *shn* func-

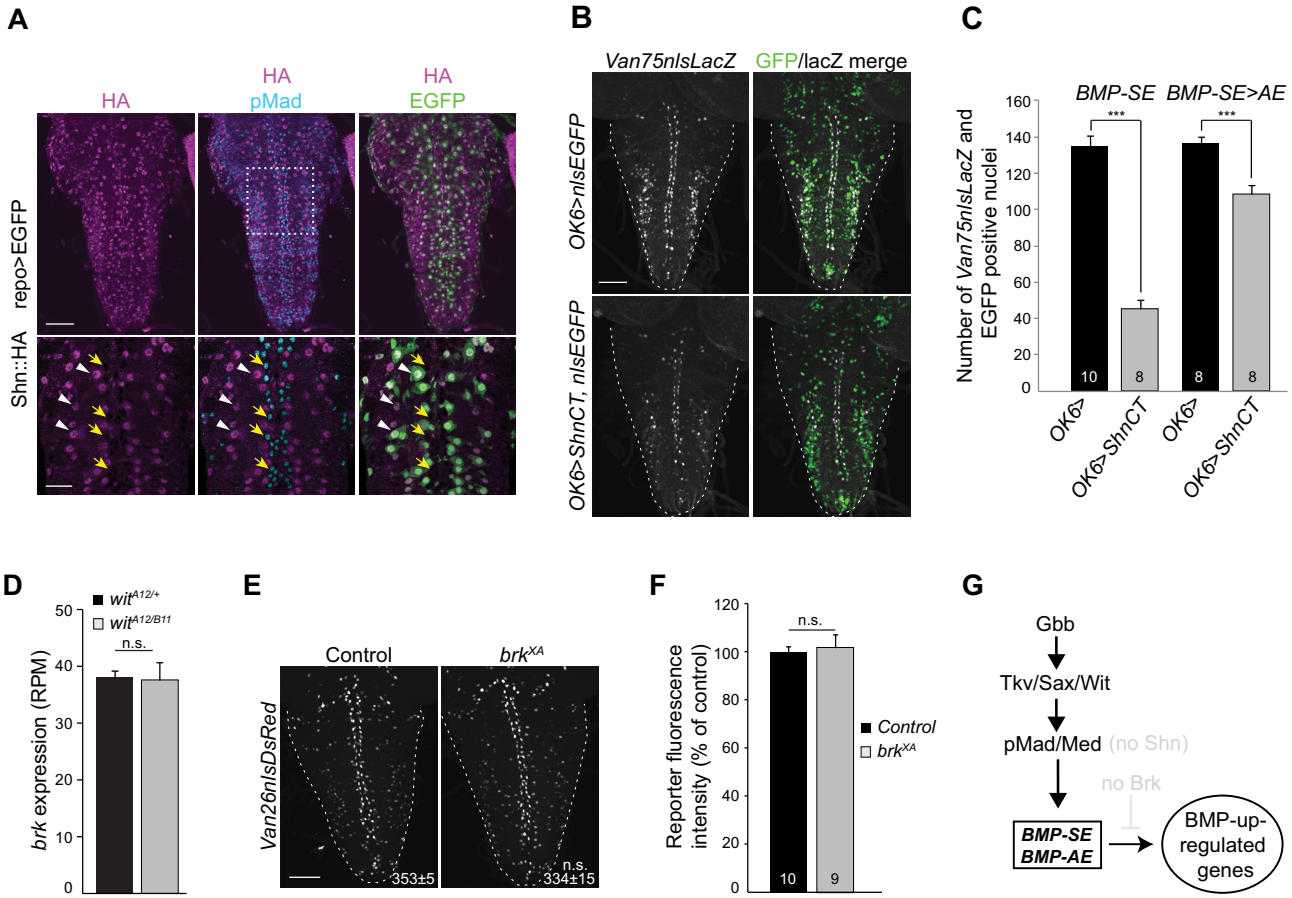

Figure 5. (**A**) Expression of an endogenous HA-tagged *shn* (*shn::HA*) allele (anti-HA immunolabeling) is restricted to *repo*-positive glia (green, white arrowheads) and neurons with no BMP signaling as revealed by the absence of pMad co-staining (blue, yellow arrows). (**B**) Reporter activity (anti-nuclear β-gal immunoreactivity) driven from the *wit*-responsive genomic fragment *Van75* with a *BMP-SE* in control and ShnCT misexpressing motor neurons. (**C**) Quantification of reporter activity loss of the Van75 genomic fragment containing either a wildtype *BMP-SE* or a converted *BMP-SE > AE* motif. The number of nuclei per VNC that are positive for EGFP and the *Van75* reporter is represented by mean ± SEM. Misexpression of ShnCT strongly downregulated the activity of the reporter containing the *BMP-SE*, but not with the *BMP-AE*. (**D**) *Brk* transcription is not altered in *wit* null VNCs. The RPM (reads per million) per biological replicate is represented by the mean ± SEM. $n = 4$ biological replicates for each RNA-seq experimental condition. (**E**) Nuclear DsRed reporter expression driven from the *wit*-responsive *Van26* reporter containing a *BMP-AE* in control and brk^{XA} mutants. The mean ± SEM number of nuclei per VNC expressing the reporter is indicated (inset). (**F**) Quantification of fluorescence intensities per VNC for genotypes shown in panel (E) is represented by mean ± SEM. The activity of the *Van26* reporter is not altered in brk^{XA}. (**G**) In this model, the *BMP-AE* and *BMP-SE* mediate the direct upregulation of BMP target genes by BMP signaling in motor neurons, in the absence of Brk and Shn (light gray). ***$P < 0.001$; n.s., not significant (two-sided unequal variance Student's *t*-test for C,E,F and Wald test, *P*-value adjusted with Benjamini–Hochberg for D) with $n = 8$–10 VNCs per genotype. Scale bars of panels A,B,E: 50 μm; A, magnification: 25 μm.

tion, in contrast to most other *Drosophila* tissues analyzed to date (Figure 5G).

*BMP-RE*s mediate BMP-upregulation of critical synaptic genes

We then wished to dissect the contribution of BMP signaling and both *BMP-RE* motif types to the regulation of synaptic genes controlling BMP-dependent synaptic functions. To this end, we focused our attention on three BMP-upregulated genes: *brp*, *cg7781* and *cg14274*. *Brp* encodes a presynaptic active zone scaffolding protein regulating synaptic neurotransmission and plasticity (56,57). The *brp* locus contains a single conserved *BMP-SE* motif that is *wit*-responsive in reporter assays (Figures 6A and 3E, *Van65*). *Cg7781* and *cg14274* encode predicted glycosylphosphatidylinositol-anchored (GPI) proteins with unknown function, which are related to the Ly6 genes *qvr* and *twit*, both controlling neurotransmission in *Drosophila* (14,58,59). *Cg7781* and *cg14274* are organized in a gene cluster (Figure 6E) that contains four conserved *BMP-AE*s mediating BMP-signaling in reporter assays (10).

Using a CRISPR/Cas9-based genome editing approach, we generated two alleles at the *brp BMP-SE* motif; a mutant allele in which the *BMP-SE* was edited to prevent pMad/Med binding, and a control allele that did not modify the *BMP-SE* but controlled for the PAM site mutations (Supplementary Figure S6). We analyzed the consequence on Brp expression at the larval NMJ by anti-Brp immunolabeling. Mutation of the *BMP-SE* motif resulted in a strong loss of Brp immunoreactivity at NMJ boutons (Figure 6B–D), supporting a role for the *BMP-SE* in mediating BMP-upregulation of this gene.

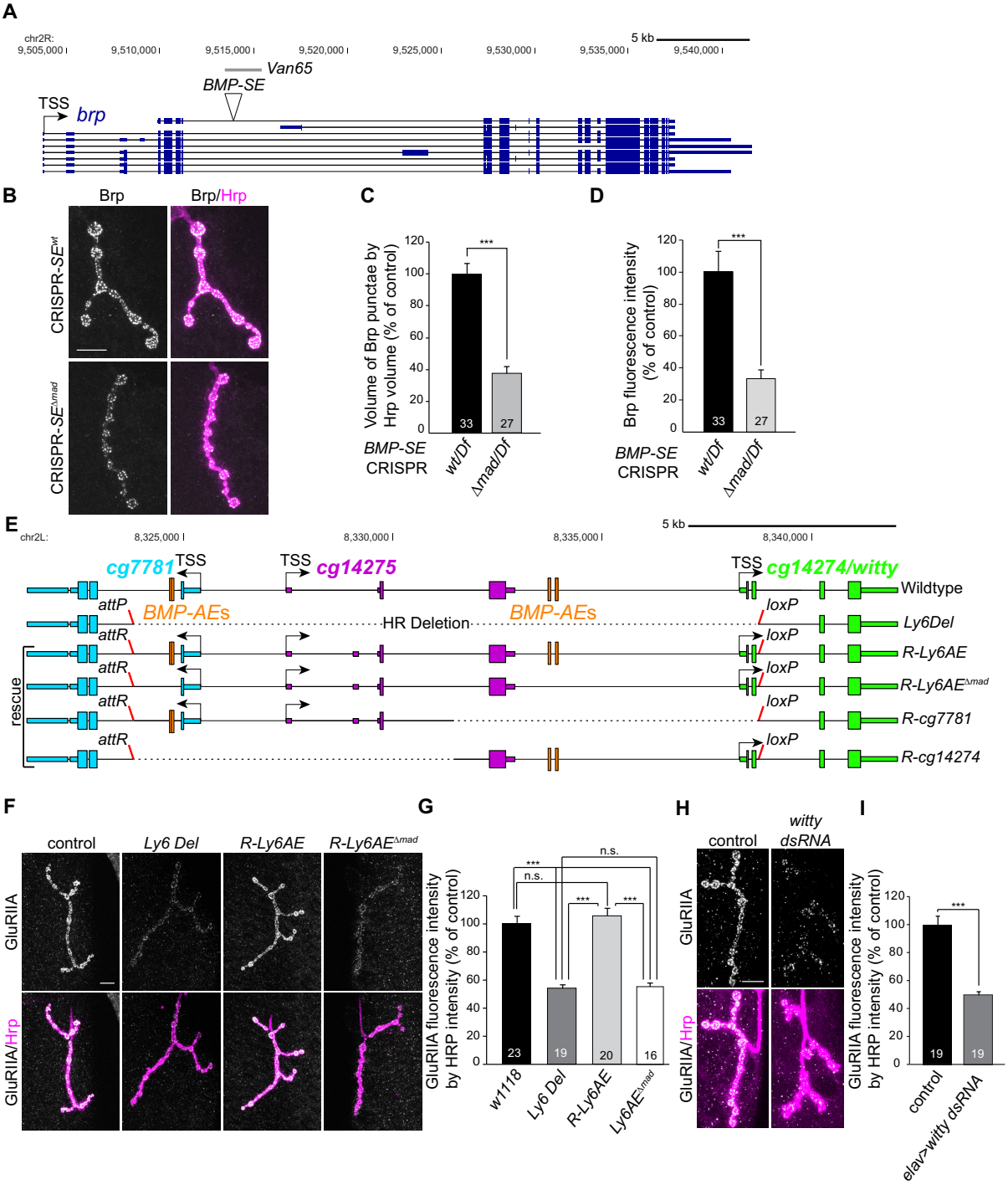

Figure 6. (**A**) Annotated UCSC genome browser image showing the *bruchpilot (brp*) locus with the *BMP-SE* and the *wit*-responsive genomic fragment used for reporter analysis. (**B**) Anti-Brp (gray) immunoreactivity at NMJ4 in wandering third instar larvae for which the *BMP-SE* is either wild-type or mutated to prevent pMad binding (ΔMad). Neurons are labeled by anti-HRP (magenta). These *BMP-SE* alleles are hemizygous over a genomic deficiency that encompasses the *brp* locus. (**C**, **D**) Quantification of Brp punctae volume (C) and intensity (D) reduction in *BMP-SE* mutants is represented by mean ± SEM. ***$P < 0.001$ (two-sided Wilcoxon rank-sum test). (**E**) Annotated UCSC genome browser image showing the *Ly6* gene locus with the four *BMP-AE*s, the region deleted (HR Deletion) in the Ly6 allele (*Ly6Del*), and the four genomic rescues in which the locus was replaced by either the wild-type sequence (*R-Ly6AE*), the wild-type sequence with mutations in the four *BMP-AE*s (*R-Ly6AE*$^{\Delta Mad}$), or a partial fragment rescuing either *cg7781* (*R-cg7781*) or *cg14274* (*R-cg14274*). The *attP* and *loxP* sites used for genome engineering are shown. (**F**) Representative NMJ4 immunostained for GluRIIA (gray) shown for controls, *Ly6Del* mutants, and in *R-Ly6AE* and *R-Ly6AE*$^{\Delta Mad}$ rescue. Anti-HRP is magenta. (**G**) Immunofluorescence intensities for genotypes shown in panel (F) are represented by mean ± SEM. The loss of anti-GluRIIA immunoreactivity in *Ly6Del* mutants is rescued in *R-Ly6AE*, but not in *R-Ly6AE*$^{\Delta Mad}$, ***$P < 0.001$, n.s., not significant (one-way ANOVA with post-hoc Tukey HSD test). (**H**) Representative NMJ4 immunostained for GluRIIA following neuronal RNAi knockdown of *witty* using the *elav-Gal4* driver. (**I**) Quantification of GluRIIA immunofluorescence after RNAi knockdown of neuronal *witty*. ***$P < 0.001$ (two-sided unequal variance Student's *t*-test). Scale bars of panels B,F,H: 10 μm.

To examine the function of Ly6 genes and their BMP-dependent upregulation by the *BMP-AE* motif, we used homologous recombination to delete a ∼15 kb region including the four *BMP-AE*s and the first coding exons of *cg7781* and *cg14274*. We replaced this region with an *attP* and a *loxP* site (*Ly6Del*) to target wild-type or modified sequences of the *Ly6* genes cluster at its endogenous locus (Figure 6E). This deletion also includes the *wit*-unresponsive Ly6 gene *cg14275* (Figure 6E and data not shown). *Ly6Del* mutants were viable and fertile, allowing us to examine phenotypes at the larval NMJ. Examining wandering third instar NMJ4, we observed a dramatic reduction of postsynaptic glutamate receptor subunit IIA (GluRIIA) in *Ly6Del* mutants (Figure 6F and G). The loss of GluRIIA was specific, since the levels of the postsynaptic marker, Discs Large (Dlg), and the active zone scaffolding protein, Bruchpilot (Brp), remained unaffected (Supplementary Figure S7A and B). To identify which of the Ly6 genes contribute to this phenotype, we examined GluRIIA in *Ly6Del* mutant NMJs rescued with two non-overlapping wild-type genomic fragments that encompass either cg7781 (*R-cg7781*) or *cg14274* (*R-cg14274*) (Figure 6E). We found that *cg14274*, but not *cg7781*, is required for GluRIIA at NMJ4 (Supplementary Figure S7C). To then test if presynaptic expression of *cg14274* regulates postsynaptic GluRIIA at the NMJ, we expressed a dsRNA against *cg14274* under the control of the *elav-Gal4* pan-neuronal driver. We observed a strong reduction of GluRIIA (Figure 6H and I) at NMJ4, indicating that neuronal *cg14274* expression controls the accumulation of GluRIIA at the post-synapse in muscle. By virtue of its function at the synapse, we named the *cg14274* gene *without maturity* (*witty*). Finally, to test if the *BMP-AE* motifs near the *witty* locus mediate BMP-dependent upregulation of *witty* in motor neurons to control postsynaptic GluRIIA, we mutated the four *BMP-AE*s in the Ly6 genes cluster (Figure 6E). Strikingly, this phenocopied the loss of GluRIIA observed in *Ly6Del* mutant NMJ4 (Figure 6F and G). Therefore, the *BMP-AEs* mediate the BMP-dependent upregulation of *witty* transcription in motor neurons to control GluRIIA accumulation in the muscle at the NMJ.

Taken together, these data demonstrate that both motifs, the *BMP-AE* and the *BMP-SE*, mediate widespread direct BMP-dependent upregulation of genes critical for synaptic maturation (Figure 7).

DISCUSSION

In this study, we identified a network of *wit*-responsive genes in *Drosophila* motor neurons, with an overrepresentation of upregulated genes involved in neurotransmission. We also found adjacent candidate *cis*-regulatory *BMP-RE*s for many of these genes. This suggests that BMP signaling primarily operates directly to upregulate a network of presynaptic genes to promote motor neuron maturation. Notably, we discovered that *BMP-SE* motifs operate as activators in motor neurons, and that the Shn/Brk de-repression pathway is absent, revealing a unique regulatory mechanism for BMP gene regulation in these cells. Next, by *BMP-RE* mutagenesis we demonstrated the role of direct BMP-dependent regulation of *brp* and the novel gene *witty*, thereby providing mechanistic insight into the contribution of retrograde BMP signaling to synaptic maturation. Considering that neurotransmission requires continuous BMP-dependent regulation and NMJ growth appears to be only BMP-dependent during early developmental time points (12), it will be interesting to monitor BMP-dependent gene expression through embryonic and larval stages after modulating BMP signaling components and activity levels in motor neurons. Furthermore, the direct BMP-dependent regulation of a large fraction of the gene network we have identified raises the possibility that BMP signaling may be involved in scalable, fast transcriptional responses to perturbations at the growing NMJ. While such mechanisms remain undemonstrated, we believe that future efforts to monitor the dynamics of BMP-regulated target gene transcription will be facilitated by our identification of direct BMP target genes and their BMP-responsive *cis*-regulatory elements.

Our findings suggest that the gene network identified here orchestrates neurotransmission and maturation at the *Drosophila* NMJ. We speculate that orthologs of many of these genes operate within related networks to control similar functions in vertebrate synapses. To expand on this, we examined if any of the neuronal genes upregulated by BMP signaling are disease relevant. Through highly stringent orthology and disease association searches, we found that 77 BMP-upregulated genes have a human gene ortholog strongly implicated in a neurological disorder. Interestingly, among those 77 genes, the ortholog of fly *Reticulon-like 1* (Reticulon 2; RTN2) is implicated in Hereditary Spastic Paraplegias (HSPs) (60). Moreover, deregulation of TGFβ/BMP signaling has also been implicated in HSPs (61–63); thus, our work suggests a relevant link between RTN2 and the TGFβ/BMP signaling pathway in HSP.

A notable finding in our study is that the *BMP-SE* operates as an activator in motor neurons. Thus, this motif does not operate as a strict silencer in *Drosophila*, but as a context-dependent dichotomous *cis*-regulatory element, depending on the tissue and the presence of Shn. Studies aimed at identifying BMP-responsive *cis*-regulatory elements in vertebrates have revealed that both *BMP-AE* and *BMP-SE*-type motif sequences are present. Interestingly, *BMP-SE*-type motifs seem to operate as strict activators in vertebrates (64,65), with Shn orthologs having a co-activator function (65,66). This observation and our findings that the *BMP-SE* motif operates as an activator in *Drosophila* motor neurons can be reconciled from an evolutionary perspective, given evidence that the CNS of both vertebrates and invertebrates share a monophyletic origin and is patterned by BMP signaling (67,68). Although the role of the BMP signaling pathway in patterning the trunk CNS along the dorso-ventral axis of animals is conserved, BMP-dependent target gene regulation is often reversed. For example, in the dorsal neuroectoderm, expression of *Drosophila msx* and zebrafish *msxB* genes are both BMP-regulated; through a *BMP-SE* motif that mediates silencing in *Drosophila* and a relaxed *BMP-SE* motif that mediates activation in zebrafish (69). Therefore, we speculate that while *BMP-AE* and *BMP-SE* motifs are activators by default, the latter motif was subsequently recruited to the repression of *brk* and other genes in numerous tissues in *Drosophila* (20,21,23–26). In contrast, in tissues where

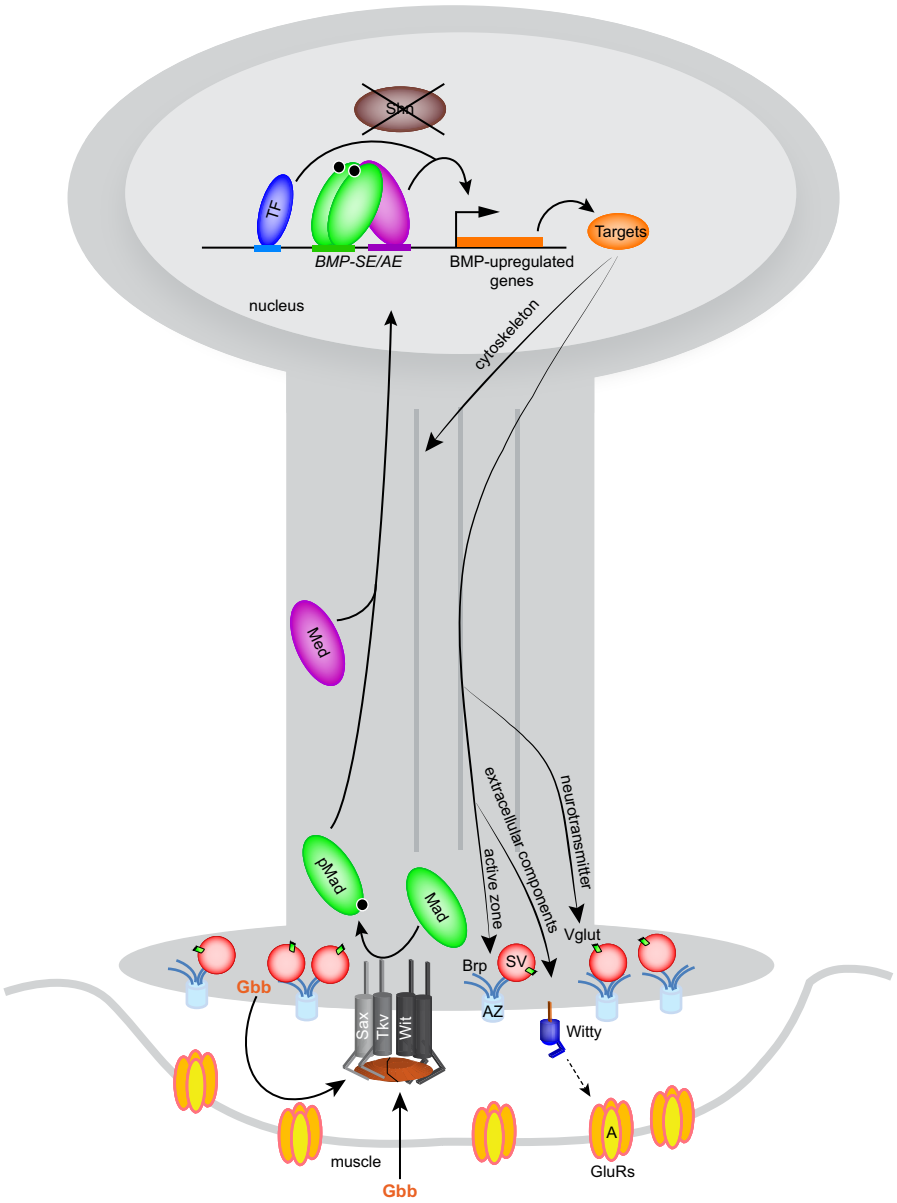

Figure 7. In this model, the BMP ligand Gbb is secreted by muscle cells and motor neurons to bind a tetrameric complex of Sax-Tkv/Wit, the type I and type II BMP receptor kinases. Upon receptor activation, cytoplasmic Mad is phosphorylated by Tkv-Sax and binds the co-Smad Med to accumulate in the motor neuron nucleus. In the absence of the corepressor Shn, the activated pMad/Med complex binds *BMP-AE* and *BMP-SE* to activate, with additional input from other transcription factors, a battery of target genes to regulate neuronal function such as neurotransmitter transport, active zone scaffolding, cytoskeleton organization and postsynaptic GluRIIA clustering.

BMP-dependent regulation of *brk* is absent, such as in *Drosophila* motor neurons, or in vertebrates where no *brk* gene is present, the *BMP-SE* retained its ancestral activator role.

By validating the function of *BMP-REs* that upregulate *brp* and *witty,* we not only demonstrate that our approach is efficient at identifying direct target genes involved in BMP-dependent synaptic functions but also provide a framework for the experimental dissection of the discrete contribution of BMP signaling to the expression and function of those genes at the NMJ. Previous work reported that Brp-positive active zones number and density was strongly reduced at the NMJ in *gbb*, *wit* and antimorphic Mad^{1} mutants (12,70). Moreover, inhibition of BMP-dependent transcription in third instar larvae led to rapid loss of active zone density, which correlates with the observed loss of competence for presynaptic homeostatic plasticity after BMP blockade (7,12). We now provide mechanistic evidence for these observations by showing that *brp* is directly BMP-upregulated. This may explain how persistent retrograde BMP signaling and transcriptional activity are required to maintain active zone integrity (7,12).

Our findings demonstrate that canonical BMP-dependent upregulation of *witty* is required for postsynaptic GluRIIA accumulation at the NMJ but does not rule out additional postsynaptic functions for *witty*.

While these data are consistent with the observation that postsynaptic GluRIIA is severely reduced in *wit* and *mad*^{1} mutants (71–73), they do contrast with recent reports that a non-canonical BMP signaling pathway dependent on synaptic pMad also regulates GluRIIA at the NMJ (71). Therefore, these canonical and non-canonical pathways may indeed function as non-redundant BMP-dependent mechanisms. To expand on such a model, we suggest that synaptic pMad may allow for acute, short-term compensatory responses, whereas the pMad-dependent transcriptional mechanism may offer a longer-term consolidation response. Future experiments aimed at defining the underlying mechanisms regulated by *witty* will be critical to understanding how presynaptic retrograde BMP signaling controls postsynaptic maturation.

In conclusion, the identification of BMP-activated genes and their *BMP-RE*s facilitates the discovery of novel synaptic genes, as well as the dissection of how BMP-dependent transcriptional regulation of target genes contributes to NMJ function. We anticipate that our approach will facilitate the disentanglement of transcriptional versus synaptic roles for BMP signaling at the NMJ.

DATA AVAILABILITY

Raw numerical data used to generate graphs can be found in Supplementary Table S5.

SUPPLEMENTARY DATA

Supplementary Data are available at NAR Online.

ACKNOWLEDGEMENTS

We are very grateful to Dr Anaïs Bardet and Dr Alexander Stark for performing the motif confidence analysis for the *BMP-SE* and also to Stephanie Huynh for helping to generate the *Ly6Del* mutant at the initial stage of the project. We thank members of the Allan laboratory and Tim O'Connor for insightful discussion and critical reading of the manuscript. We also thank Yang Hong, Markus Affolter, Allen Laughon and the Bloomington and VDRC *Drosophila* Stock Centers, the *Drosophila* Genomics Resource Center P[acman] Resources for fly stocks and molecular reagents.

Author contributions: R.V. and D.W.A. conceived and designed the experiments. R.V. performed most of the experiments. M.M. generated the wildtype and mutant CRISPR alleles of the *BMP-SE* in the *brp* locus, performed the immunostaining of Brp at NMJ4 with assistance from R.V. and quantified the data. T.L. performed the EMSA experiments. G.P. and C.-M.E. generated the *Shn::HA* and *Brk::HA* alleles. S.F. and R.V. performed the bioinformatics analysis. S.M.-G. quantified the expression of the molecular markers at Ly6 genes cluster mutant NMJ. A.P.H. and G.K. discovered the loss of GluRIIA in the *Ly6Del* mutant. R.V., A.C. and S.L. generated mutant versions of the reporter constructs. R.V., M.M., T.L., S.F., S.M.-G, A.C., S.L. and D.W.A. analyzed data. R.V. generated the figures. R.V. and D.W.A. wrote the manuscript.

FUNDING

Canadian Institutes of Health Research (CIHR) [F16-01394, F20-04798 to D.W.A.]; Deutsche Forschungsgemeinschaft [EXC-2189, Project ID: 390939984 to G.P.]; National Institutes of Health (NIH) [R01NS082793 to A.P.H]. Funding for open access charge: CIHR [F20-04798].
Conflict of interest statement. None declared.

REFERENCES

1. Sanyal,S., Kim,S.M. and Ramaswami,M. (2004) Retrograde regulation in the CNS; neuron-specific interpretations of TGF-beta signaling. *Neuron*, **41**, 845–848.
2. Meyers,E.A. and Kessler,J.A. (2017) TGF-β family signaling in neural and neuronal differentiation, development, and function. *Cold Spring Harb. Perspect. Biol.*, **9**, a022244.
3. Bayat,V., Jaiswal,M. and Bellen,H.J. (2011) The BMP signaling pathway at the drosophila neuromuscular junction and its links to neurodegenerative diseases. *Curr. Opin. Neurobiol.*, **21**, 182–188.
4. Kashima,R. and Hata,A. (2018) The role of TGF-β superfamily signaling in neurological disorders. *Acta Biochim. Biophys. Sin. (Shanghai)*, **50**, 106–120.
5. Marqués,G., Bao,H., Haerry,T.E., Shimell,M.J., Duchek,P., Zhang,B. and O'Connor,M.B. (2002) The drosophila BMP type II receptor wishful thinking regulates neuromuscular synapse morphology and function. *Neuron*, **33**, 529–543.
6. Aberle,H., Haghighi,A.P., Fetter,R.D., McCabe,B.D., Magalhães,T.R. and Goodman,C.S. (2002) Wishful thinking encodes a BMP type II receptor that regulates synaptic growth in drosophila. *Neuron*, **33**, 545–558.
7. Goold,C.P. and Davis,G.W. (2007) The BMP ligand gbb gates the expression of synaptic homeostasis independent of synaptic growth control. *Neuron*, **56**, 109–123.
8. Rawson,J.M., Lee,M., Kennedy,E.L. and Selleck,S.B. (2003) Drosophila neuromuscular synapse assembly and function require the TGF-beta type i receptor saxophone and the transcription factor mad. *J. Neurobiol.*, **55**, 134–150.
9. Smith,R.B., Machamer,J.B., Kim,N.C., Hays,T.S. and Marqués,G. (2012) Relay of retrograde synaptogenic signals through axonal transport of BMP receptors. *J. Cell. Sci.*, **125**, 3752–3764.
10. Vuilleumier,R., Lian,T., Flibotte,S., Khan,Z.N., Fuchs,A., Pyrowolakis,G. and Allan,D.W. (2019) Retrograde BMP signaling activates neuronal gene expression through widespread deployment of a conserved BMP-responsive cis-regulatory activation element. *Nucleic Acids Res.*, **47**, 679–699.
11. McCabe,B.D., Hom,S., Aberle,H., Fetter,R.D., Marques,G., Haerry,T.E., Wan,H., O'Connor,M.B., Goodman,C.S. and Haghighi,A.P. (2004) Highwire regulates presynaptic BMP signaling essential for synaptic growth. *Neuron*, **41**, 891–905.
12. Berke,B., Wittnam,J., McNeill,E., Van Vactor,D.L. and Keshishian,H. (2013) Retrograde BMP signaling at the synapse: a permissive signal for synapse maturation and activity-dependent plasticity. *J. Neurosci.*, **33**, 17937–17950.
13. Ball,R.W., Warren-Paquin,M., Tsurudome,K., Liao,E.H., Elazzouzi,F., Cavanagh,C., An,B.S., Wang,T.T., White,J.H. and Haghighi,A.P. (2010) Retrograde BMP signaling controls synaptic growth at the NMJ by regulating trio expression in motor neurons. *Neuron*, **66**, 536–549.
14. Kim,N.C. and Marqués,G. (2012) The Ly6 neurotoxin-like molecule target of wit regulates spontaneous neurotransmitter release at the developing neuromuscular junction in drosophila. *Dev. Neurobiol.*, **72**, 1541–1558.
15. Affolter,M., Pyrowolakis,G., Weiss,A. and Basler,K. (2008) Signal-induced repression: the exception or the rule in developmental signaling?*Dev. Cell.*, **15**, 11–22.
16. Barolo,S. and Posakony,J.W. (2002) Three habits of highly effective signaling pathways: principles of transcriptional control by developmental cell signaling. *Genes Dev.*, **16**, 1167–1181.
17. Campbell,G. and Tomlinson,A. (1999) Transducing the dpp morphogen gradient in the wing of drosophila: regulation of dpp targets by brinker. *Cell*, **96**, 553–562.

18. Minami,M., Kinoshita,N., Kamoshida,Y., Tanimoto,H. and Tabata,T. (1999) Brinker is a target of dpp in drosophila that negatively regulates dpp-dependent genes. *Nature*, **398**, 242–246.
19. Jaźwińska,A., Kirov,N., Wieschaus,E., Roth,S. and Rushlow,C. (1999) The drosophila gene brinker reveals a novel mechanism of dpp target gene regulation. *Cell*, **96**, 563–573.
20. Müller,B., Hartmann,B., Pyrowolakis,G., Affolter,M. and Basler,K. (2003) Conversion of an extracellular dpp/BMP morphogen gradient into an inverse transcriptional gradient. *Cell*, **113**, 221–233.
21. Pyrowolakis,G., Hartmann,B., Müller,B., Basler,K. and Affolter,M. (2004) A simple molecular complex mediates widespread BMP-induced repression during drosophila development. *Dev. Cell.*, **7**, 229–240.
22. Stathopoulos,A. and Levine,M. (2005) Localized repressors delineate the neurogenic ectoderm in the early drosophila embryo. *Dev. Biol.*, **280**, 482–493.
23. Beira,J.V., Springhorn,A., Gunther,S., Hufnagel,L., Pyrowolakis,G. and Vincent,J.P. (2014) The dpp/TGFβ-dependent corepressor schnurri protects epithelial cells from JNK-induced apoptosis in drosophila embryos. *Dev. Cell.*, **31**, 240–247.
24. Vuilleumier,R., Springhorn,A., Patterson,L., Koidl,S., Hammerschmidt,M., Affolter,M. and Pyrowolakis,G. (2010) Control of dpp morphogen signalling by a secreted feedback regulator. *Nat. Cell Biol.*, **12**, 611–617.
25. Chen,D. and McKearin,D.M. (2003) A discrete transcriptional silencer in the bam gene determines asymmetric division of the drosophila germline stem cell. *Development*, **130**, 1159–1170.
26. Chen,D. and McKearin,D. (2003) Dpp signaling silences bam transcription directly to establish asymmetric divisions of germline stem cells. *Curr. Biol.*, **13**, 1786–1791.
27. Chen,H., Xu,Z., Mei,C., Yu,D. and Small,S. (2012) A system of repressor gradients spatially organizes the boundaries of bicoid-dependent target genes. *Cell*, **149**, 618–629.
28. Deignan,L., Pinheiro,M.T., Sutcliffe,C., Saunders,A., Wilcockson,S.G., Zeef,L.A., Donaldson,I.J. and Ashe,H.L. (2016) Regulation of the BMP signaling-responsive transcriptional network in the drosophila embryo. *PLoS Genet*., **12**, e1006164.
29. Thomas,P.D., Kejariwal,A., Campbell,M.J., Mi,H., Diemer,K., Guo,N., Ladunga,I., Ulitsky-Lazareva,B., Muruganujan,A., Rabkin,S. *et al.* (2003) PANTHER: a browsable database of gene products organized by biological function, using curated protein family and subfamily classification. *Nucleic Acids Res*., **31**, 334–341.
30. Mi,H., Muruganujan,A. and Thomas,P.D. (2013) PANTHER in 2013: modeling the evolution of gene function, and other gene attributes, in the context of phylogenetic trees. *Nucleic Acids Res*., **41**, D377–D86.
31. Huang da,W., Sherman,B.T. and Lempicki,R.A. (2009) Bioinformatics enrichment tools: paths toward the comprehensive functional analysis of large gene lists. *Nucleic Acids Res*., **37**, 1–13.
32. Huang da,W., Sherman,B.T. and Lempicki,R.A. (2009) Systematic and integrative analysis of large gene lists using DAVID bioinformatics resources. *Nat. Protoc.*, **4**, 44–57.
33. Szklarczyk,D., Gable,A.L., Lyon,D., Junge,A., Wyder,S., Huerta-Cepas,J., Simonovic,M., Doncheva,N.T., Morris,J.H., Bork,P. *et al.* (2019) STRING v11: Protein-protein association networks with increased coverage, supporting functional discovery in genome-wide experimental datasets. *Nucleic Acids Res*., **47**, D607–D613.
34. Shannon,P., Markiel,A., Ozier,O., Baliga,N.S., Wang,J.T., Ramage,D., Amin,N., Schwikowski,B. and Ideker,T. (2003) Cytoscape: a software environment for integrated models of biomolecular interaction networks. *Genome Res*., **13**, 2498–2504.
35. Hu,Y., Flockhart,I., Vinayagam,A., Bergwitz,C., Berger,B., Perrimon,N. and Mohr,S.E. (2011) An integrative approach to ortholog prediction for disease-focused and other functional studies. *BMC Bioinformatics*, **12**, 357–2105.
36. Yates,A.D., Achuthan,P., Akanni,W., Allen,J., Allen,J., Alvarez-Jarreta,J., Amode,M.R., Armean,I.M., Azov,A.G., Bennett,R. *et al.* (2020) Ensembl 2020. *Nucleic Acids Res*., **48**, D682–D688.
37. Bauer-Mehren,A., Rautschka,M., Sanz,F. and Furlong,L.I. (2010) DisGeNET: a cytoscape plugin to visualize, integrate, search and analyze gene-disease networks. *Bioinformatics*, **26**, 2924–2926.
38. Bauer-Mehren,A., Bundschus,M., Rautschka,M., Mayer,M.A., Sanz,F. and Furlong,L.I. (2011) Gene-disease network analysis reveals functional modules in mendelian, complex and environmental diseases. *PLoS One*, **6**, e20284.
39. Piñero,J., Saüch,J., Sanz,F. and Furlong,L.I. (2021) The DisGeNET cytoscape app: exploring and visualizing disease genomics data. *Comput. Struct. Biotechnol. J.*, **19**, 2960–2967.
40. Chen,E.Y., Tan,C.M., Kou,Y., Duan,Q., Wang,Z., Meirelles,G.V., Clark,N.R. and Ma'ayan,A. (2013) Enrichr: interactive and collaborative HTML5 gene list enrichment analysis tool. *BMC Bioinformatics*, **14**, 128–2105.
41. Kuleshov,M.V., Jones,M.R., Rouillard,A.D., Fernandez,N.F., Duan,Q., Wang,Z., Koplev,S., Jenkins,S.L., Jagodnik,K.M., Lachmann,A. *et al.* (2016) Enrichr: a comprehensive gene set enrichment analysis web server 2016 update. *Nucleic Acids Res*., **44**, W90–W97.
42. Xie,Z., Bailey,A., Kuleshov,M.V., Clarke,D.J.B., Evangelista,J.E., Jenkins,S.L., Lachmann,A., Wojciechowicz,M.L., Kropiwnicki,E., Jagodnik,K.M. *et al.* (2021) Gene set knowledge discovery with enrichr. *Curr. Protoc.*, **1**, e90.
43. Markstein,M., Markstein,P., Markstein,V. and Levine,M.S. (2002) Genome-wide analysis of clustered dorsal binding sites identifies putative target genes in the drosophila embryo. *Proc. Natl. Acad. Sci. U.S.A.*, **99**, 763–768.
44. Adams,M.D., Celniker,S.E., Holt,R.A., Evans,C.A., Gocayne,J.D., Amanatides,P.G., Scherer,S.E., Li,P.W., Hoskins,R.A., Galle,R.F. *et al.* (2000) The genome sequence of drosophila melanogaster. *Science*, **287**, 2185–2195.
45. Hoskins,R.A., Carlson,J.W., Wan,K.H., Park,S., Mendez,I., Galle,S.E., Booth,B.W., Pfeiffer,B.D., George,R.A., Svirskas,R. *et al.* (2015) The release 6 reference sequence of the drosophila melanogaster genome. *Genome Res*., **25**, 445–458.
46. Port,F., Chen,H.M., Lee,T. and Bullock,S.L. (2014) Optimized CRISPR/cas tools for efficient germline and somatic genome engineering in drosophila. *Proc. Natl. Acad. Sci. U.S.A.*, **111**, E2967–E2976.
47. Baena-Lopez,L.A., Alexandre,C., Mitchell,A., Pasakarnis,L. and Vincent,J.P. (2013) Accelerated homologous recombination and subsequent genome modification in drosophila. *Development*, **140**, 4818–4825.
48. Gratz,S.J., Ukken,F.P., Rubinstein,C.D., Thiede,G., Donohue,L.K., Cummings,A.M. and O'Connor-Giles,K.M. (2014) Highly specific and efficient CRISPR/Cas9-catalyzed homology-directed repair in drosophila. *Genetics*, **196**, 961–971.
49. Huang,J., Zhou,W., Watson,A.M., Jan,Y.N. and Hong,Y. (2008) Efficient ends-out gene targeting in drosophila. *Genetics*, **180**, 703–707.
50. Huang,J., Zhou,W., Dong,W., Watson,A.M. and Hong,Y. (2009) From the cover: directed, efficient, and versatile modifications of the drosophila genome by genomic engineering. *Proc. Natl. Acad. Sci. U.S.A.*, **106**, 8284–8289.
51. Zhou,W., Huang,J., Watson,A.M. and Hong,Y. (2012) W::Neo: a novel dual-selection marker for high efficiency gene targeting in drosophila. *PLoS One*, **7**, e31997.
52. Marx,A., Backes,C., Meese,E., Lenhof,H.P. and Keller,A. (2016) EDISON-WMW: exact dynamic programing solution of the wilcoxon-mann-whitney test. *Genom. Proteom. Bioinf.*, **14**, 55–61.
53. Weiss,A., Charbonnier,E., Ellertsdóttir,E., Tsirigos,A., Wolf,C., Schuh,R., Pyrowolakis,G. and Affolter,M. (2010) A conserved activation element in BMP signaling during drosophila development. *Nat. Struct. Mol. Biol.*, **17**, 69–76.
54. Kheradpour,P., Stark,A., Roy,S. and Kellis,M. (2007) Reliable prediction of regulator targets using 12 drosophila genomes. *Genome Res*., **17**, 1919–1931.
55. Gafner,L., Dalessi,S., Escher,E., Pyrowolakis,G., Bergmann,S. and Basler,K. (2013) Manipulating the sensitivity of signal-induced repression: quantification and consequences of altered brinker gradients. *PLoS One*, **8**, e71224.
56. Wagh,D.A., Rasse,T.M., Asan,E., Hofbauer,A., Schwenkert,I., Dürrbeck,H., Buchner,S., Dabauvalle,M.C., Schmidt,M., Qin,G. *et al.* (2006) Bruchpilot, a protein with homology to ELKS/CAST, is required for structural integrity and function of synaptic active zones in drosophila. *Neuron*, **49**, 833–844.
57. Kittel,R.J., Wichmann,C., Rasse,T.M., Fouquet,W., Schmidt,M., Schmid,A., Wagh,D.A., Pawlu,C., Kellner,R.R., Willig,K.I. *et al.*

(2006) Bruchpilot promotes active zone assembly, Ca2+ channel clustering, and vesicle release. *Science*, **312**, 1051–1054.
58. Wang,J.W., Humphreys,J.M., Phillips,J.P., Hilliker,A.J. and Wu,C.F. (2000) A novel leg-shaking drosophila mutant defective in a voltage-gated K(+)current and hypersensitive to reactive oxygen species. *J. Neurosci.*, **20**, 5958–5964.
59. Koh,K., Joiner,W.J., Wu,M.N., Yue,Z., Smith,C.J. and Sehgal,A. (2008) Identification of SLEEPLESS, a sleep-promoting factor. *Science*, **321**, 372–376.
60. Montenegro,G., Rebelo,A.P., Connell,J., Allison,R., Babalini,C., D'Aloia,M., Montieri,P., Schüle,R., Ishiura,H., Price,J. *et al.* (2012) Mutations in the ER-shaping protein reticulon 2 cause the axon-degenerative disorder hereditary spastic paraplegia type 12. *J. Clin. Invest.*, **122**, 538–544.
61. Summerville,J.B., Faust,J.F., Fan,E., Pendin,D., Daga,A., Formella,J., Stern,M. and McNew,J.A. (2016) The effects of ER morphology on synaptic structure and function in drosophila melanogaster. *J. Cell. Sci.*, **129**, 1635–1648.
62. Wang,X., Shaw,W.R., Tsang,H.T., Reid,E. and O'Kane,C.J. (2007) Drosophila spichthyin inhibits BMP signaling and regulates synaptic growth and axonal microtubules. *Nat. Neurosci.*, **10**, 177–185.
63. Tsang,H.T., Edwards,T.L., Wang,X., Connell,J.W., Davies,R.J., Durrington,H.J., O'Kane,C.J., Luzio,J.P. and Reid,E. (2009) The hereditary spastic paraplegia proteins NIPA1, spastin and spartin are inhibitors of mammalian BMP signalling. *Hum. Mol. Genet.*, **18**, 3805–3821.
64. Javier,A.L., Doan,L.T., Luong,M., Reyes de Mochel,NS, Sun,A., Monuki,E.S. and Cho,K.W. (2012) Bmp indicator mice reveal dynamic regulation of transcriptional response. *PLoS One*, **7**, e42566.
65. Yao,L.C., Blitz,I.L., Peiffer,D.A., Phin,S., Wang,Y., Ogata,S., Cho,K.W., Arora,K. and Warrior,R. (2006) Schnurri transcription factors from drosophila and vertebrates can mediate bmp signaling through a phylogenetically conserved mechanism. *Development*, **133**, 4025–4034.
66. Jin,W., Takagi,T., Kanesashi,S.N., Kurahashi,T., Nomura,T., Harada,J. and Ishii,S. (2006) Schnurri-2 controls BMP-dependent adipogenesis via interaction with smad proteins. *Dev. Cell.*, **10**, 461–471.
67. Reichert,H. and Simeone,A. (2001) Developmental genetic evidence for a monophyletic origin of the bilaterian brain. *Philos. Trans. R. Soc. Lond. B. Biol. Sci.*, **356**, 1533–1544.
68. Mizutani,C.M. and Bier,E. (2008) EvoD/vo: the origins of BMP signalling in the neuroectoderm. *Nat. Rev. Genet.*, **9**, 663–677.
69. Esteves,F.F., Springhorn,A., Kague,E., Taylor,E., Pyrowolakis,G., Fisher,S. and Bier,E. (2014) BMPs regulate msx gene expression in the dorsal neuroectoderm of drosophila and vertebrates by distinct mechanisms. *PLoS Genet*., **10**, e1004625.
70. Hoover,K.M., Gratz,S.J., Qi,N., Herrmann,K.A., Liu,Y., Perry-Richardson,J.J., Vanderzalm,P.J., O'Connor-Giles,K.M. and Broihier,H.T. (2019) The calcium channel subunit α(2)δ-3 organizes synapses via an activity-dependent and autocrine BMP signaling pathway. *Nat. Commun.*, **10**, 5575–5019.
71. Sulkowski,M.J., Han,T.H., Ott,C., Wang,Q., Verheyen,E.M., Lippincott-Schwartz,J. and Serpe,M. (2016) A novel, noncanonical BMP pathway modulates synapse maturation at the drosophila neuromuscular junction. *PLoS Genet*., **12**, e1005810.
72. Nguyen,T.H., Han,T.H., Newfeld,S.J. and Serpe,M. (2020) Selective disruption of synaptic BMP signaling by a smad mutation adjacent to the highly conserved H2 helix. *Genetics*, **216**, 159–175.
73. Kamimura,K., Odajima,A., Ikegawa,Y., Maru,C. and Maeda,N. (2019) The HSPG glypican regulates experience-dependent synaptic and behavioral plasticity by modulating the non-canonical BMP pathway. *Cell. Rep.*, **28**, 3144–3156.